AD_____

Award Number: W81XWH-07-1-0083

TITLE: On-line Adaptive Radiation Treatment of Prostate Cancer

PRINCIPAL INVESTIGATOR: Tiezhi Zhang

CONTRACTING ORGANIZATION: William Beaumont Hospital
Royal Oak, Michigan

REPORT DATE: January 2008

TYPE OF REPORT: Annual

PREPARED FOR: U.S. Army Medical Research and Materiel Command
Fort Detrick, Maryland 21702-5012

DISTRIBUTION STATEMENT: Approved for Public Release;
Distribution Unlimited

REPORT DOCUMENTATION PAGE

Form Approved
OMB No. 0704-0188

1. REPORT DATE	2. REPORT TYPE	3. DATES COVERED
31-01-2008	Annual	1 JAN 2007 - 31 DEC 2007

4. TITLE AND SUBTITLE

On-line Adaptive Radiation Treatment of Prostate Cancer

5a. CONTRACT NUMBER

5b. GRANT NUMBER
W81XWH-07-1-0083

5c. PROGRAM ELEMENT NUMBER

6. AUTHOR(S)

Tiezhi Zhang

Email: tiezhi.zhang@beaumont.edu

5d. PROJECT NUMBER

5e. TASK NUMBER

5f. WORK UNIT NUMBER

7. PERFORMING ORGANIZATION NAME(S) AND ADDRESS(ES)

William Beaumont Hospital
Royal Oak, Michigan

8. PERFORMING ORGANIZATION REPORT NUMBER

9. SPONSORING / MONITORING AGENCY NAME(S) AND ADDRESS(ES)
U.S. Army Medical Research and Materiel Command
Fort Detrick, Maryland 21702-5012

10. SPONSOR/MONITOR'S ACRONYM(S)

11. SPONSOR/MONITOR'S REPORT NUMBER(S)

12. DISTRIBUTION / AVAILABILITY STATEMENT
Approved for Public Release; Distribution Unlimited

13. SUPPLEMENTARY NOTES

14. ABSTRACT

None provided.

15. SUBJECT TERMS
None provided.

16. SECURITY CLASSIFICATION OF:			17. LIMITATION OF ABSTRACT	18. NUMBER OF PAGES	19a. NAME OF RESPONSIBLE PERSON
a. REPORT	b. ABSTRACT	c. THIS PAGE			USAMRMC
U	U	U	UU	53	19b. TELEPHONE NUMBER *(include area code)*

Table of Contents

	Page
Introduction……..	**3**
Body……..	**3-5**
Key Research Accomplishments…….	**5**
Reportable Outcomes……	**5-6**
Conclusion……	**6**
References……	**7**
Appendices……	**8-**

RE: DOD Grant W81XWH-07-1-0083

PROGRESS REPORT SUMMARY

INTRODUCTION

Organ motion is a major uncertainty in prostate cancer treatment. In this project, we are developing online adaptive treatment that can compensate organ motion in daily treatments. The specific aims of this project are to develop the key technical components for online adaptive treatment, which include parallel deformable image registration algorithm, parallel dose calculation and plan optimization algorithms.

STUDIES AND RESULTS: YEAR 1

A. Evaluation of the benefit of online adaptive treatment for prostate cancer

We first evaluated the benefits of online treatment plan re-optimization for prostate treatment. Through the virtual treatment simulation study, we have discovered that online re-optimization is most beneficial to the patients with seminal vesicle involvement. Reduction in rectum and bladder equivalent uniform dose (EUD) has been observed as high as 20% for those patients. The results have been reported in an international conference and a manuscript has been submitted to the journal of Radiotherapy and Oncology [1].

B. Developing of parallel deformable image registration algorithm.

We have implemented an intensity-based deformable image registration algorithm on a 16-PE (processing element) Beowulf cluster. This algorithm has been used for deformable registration of various sites including the prostate. We have set up a deformable registration cluster in our clinic so that the research outcomes are utilized in the clinical treatment planning.

The robustness of deformable image registration for head and neck cases was quantitatively evaluated using multiple CT images for 10 patients with each patient having 9 daily CT images. The automatically delineated region of interests (ROIs) were compared with manual delineation which was considered as golden standards. Results showed excellent agreement between automatically and manually delineated ROIs. The results have been published in International Journal of Radiation Oncology Biology Physics[2]. The registration of head neck cone beam CT images has also been evaluated and the results will be reported in an international conference[3].

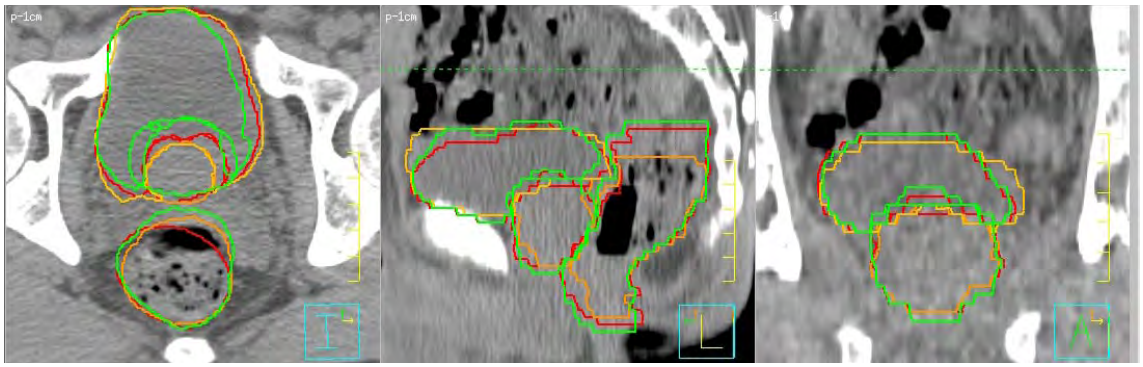

Figure 1 An example of automatic delineation of ROI in daily prostate images. (Red: reference contours, green: automatic contour, orange: manual contours).

Evaluation of prostate registration is still in progress. Figure 1 shows the results of automatic delineation of the prostate. Generally the manual contours agree with automatic contours. However, bowel gas and rectum filling frequently cause problems in deformable image registration. Currently we are working in two directions to solve this problem: (1) control patient's diet and give instruction to the patient to empty bladder and rectum before treatment; (2) create organ model and perform statistical training. Rectum balloon may be another option.

To accelerate registration speed, we have implemented parallel deformable image registration using Message Passing Interface (MPI). The speed up factor and efficiency of the parallel deformable image registration algorithms are show in Figure 2. Using a 16-PE cluster, we have achieved a speedup factor of 15. Registration of 3D CT images takes only about 2-3 mins. We expect the time can be reduced to within 30 sec with a 64-PE computer cluster. The results have been reported in an international conference[4].

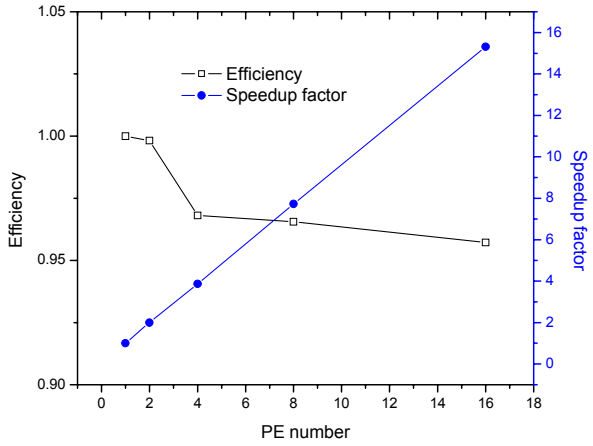

Figure 2 Benchmark results of parallel deformable image registration algorithm. Efficiency and speedup factors with different numbers of PEs.

C. Developing of parallel IMRT re-optimization algorithm.

Online re-planning requires online dose calculation and online plan re-optimization. All ROIs in prostate treatment are deep inside patient's body. Dose calculation on daily images may be very similar to the dose calculated on planning CT images. In order to prove that we have performed treatment planning studies on 10 patients with each patient has 10 daily images. The maximum target dose differences were less than 1% and most rectum and bladder dose difference is less than 5%. The results suggested that in daily adaptive treatment, it is not necessary to calculate dose on daily images. IMRT re-optimization can simply be performed using planning dose. This approach can greatly simplify the procedure of online adaptive treatment. The results have been presented in international conference[5].

We have implemented a simultaneous projection optimization algorithm for IMRT treatment plan optimization. We utilized the same DVH objective and constraint definitions as Pinnacle TPS so that the developed algorithms can be readily integrated with commercial TPS. Simultaneous projection optimization algorithm is ideal for parallel computing due to its simultaneous property. We have implemented this algorithm on a 16-PE Beowulf cluster. Message passing interface (MPI) was used in parallel programming. The scalability of a parallel algorithm is determined by the overhead communication. Our cluster uses low-cost but relatively slow Gigabyte network switches for inter-nodal communication. Figure 3 shows the benchmark results of speedup factors using this computer cluster.

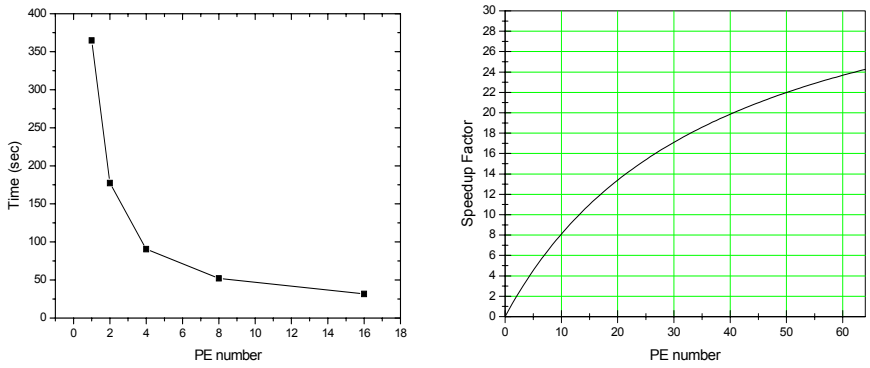

Figure 3 Parallel IMRT optimization benchmark results. Left: measured optimization time vs. number of PEs used. Right: predicted speedup factor for larger scale clusters.

The results show that the serial component of our parallel optimization algorithm is about 2.6%. Figure 3 also plotted the projected speedup factor vs. number of PE with s=0.026. One can see that the speedup factor does not increase linearly. The typical computation time of IMRT prostate treatment planning is about 5 minutes. The computation time could be reduced to about 17 sec with 32 PEs. The results will be reported in an international conference[5].

D. Interface the developed algorithm with Pinnacle treatment planning system

Pinnacle TPS allows addition of custom developed functions via plugins and scripts. The developed parallel algorithms run on a computer clusters. We have developed Pinnacle interfacing scripts for the communication between TPS and the computer cluster. So that users can easily send jobs to the clusters and review the results in Pinnacle TPS. The developed tools have been clinically implemented and utilized in clinical treatment planning.

KEY RESEACH ACCOMPLISHMENT

1. We have developed fast deformable image registration using parallel computing technique. Basing on the benchmark results, we project deformable image registration can be shorten to within 30 sec with a 64-PE computer cluster. We have also evaluated the automatic image segmentation results for various treatment sites. The algorithm shows great robustness in head and neck cases. We are further improving the algorithm to improve the succeed rate in prostate image segmentation.

2. We have developed fast IMRT optimization using parallel computing technique. We proved that online dose calculation is not necessary in online re-planning. The parallel optimization algorithm is very fast and can re-optimize a treatment plan in about 17 sec with a 32 PE computer cluster.

REPORTABLE OUTCOMES:

Peer reviewed publications:

1. Tiezhi Zhang, Yuwei Chi et al, “Automatic Delineation of Online Head-And-Neck Computed Tomography Images: Toward Online Adaptive Radiotherapy”, International Journal of Radiation Oncology, Biology and Physics 2007 68(5): 1572-8.

2. Derek Schulte, Tiezhi Zhang, "Comparison of various online IGRT strategies: The benefits of online treatment plan re-optimization", Radiotherapy and Oncology, under review.

Conference presentations:

1. D. Schulze, T. Zhang, "Techniques of Online IMRT Plan Re-Optimization for Prostate Cancer Treatments", 50th ASTRO annual conference, Boston, MA, 2008.
2. T. Zhang, *et al, "Online delineation of head and neck CT images",* 49th AAPM annual conference, Minneapolis, MN, 2007
3. T. Zhang, D. Schulze, et al, "Online Adaptive Prostate Cancer Intensity Modulated Radiation Treatment (IMRT): Method of Online Plan Re-optimization" 49th ASTRO annual conference, Los Angels, CA, 2007
4. D. Schulze, T. Zhang, et al, "Dosimetric Comparison of Various Online Adaptive Prostate Cancer Treatment Techniques", Los Angels, CA, 2007
5. T. Zhang*, et al, "Clinical Applications of 3D and 4D Deformable Image Registration for Image Guided Radiotherapy*", 48th AAPM annual conference, Orlando, FL, 2006
6. T. Zhang, *et al, "Automatic Delineation of Daily CT Images for Online Plan Adjustments: Method and Quantitative Validation",* 48th ASTRO annual conference, Philadelphia, PA, 2006
7. L. Burgess, T. Zhang*, et al, "Image Guided Radiotherapy by Online Plan Re-optimization: Studies of Dosimetric Benefits by Treatment Simulations",* 48th ASTRO annual conference, Philadelphia, PA, 2006

Degrees obtained:

1. Derek Schulze, Master of Science, Department of Medical Physics, Wayne State University, Detroit, Michigan

Funding applied for:

1. Development of Ultra Fast Intensity Modulated Arc Therapy (IMAT) Planning and Delivery Methods for Prostate Cancer Treatments, PI, Tiezhi Zhang, DOD prostate cancer research program
   In this proposal, we will develop fast treatment delivery method which can complete a treatment fraction within 1-2 mins. This method will minimize the intrafraction motion during online adaptive treatment.
2. Development of A Quasi-CBCT System for Image Guided Radiotherapy, PI, Tiezhi Zhang, NIH R21, Started on 3/1/2008
   In this proposal, we will develop a novel imaging system using a linear x-ray source and a linear detector. This imaging system may significantly improve the quality of online images, which is critically important for online ROI delineation.

CONCLUSIONS:

During the first phase of the study, we have developed various techniques for online adaptive techniques. The completed studies showed that online adaptive treatment is feasible using the developed techniques. With parallel computing technique, the computation time of online re-planning can be reduced to within 1 min.

The quality of automatic image segmentation is acceptable for some treatment sites such as head and neck. However, we also noticed that automatic image segmentation of prostate images is not always robust. We need to develop specific methods to accommodate the extreme low contrast and large deformation in prostate images. This will be a major effort in the next phase of study.

REFERENCE:

1. D Schulte, T Zhang, “Comparison of various online IGRT strategies: The benefits of online treatment plan re-optimization”, Submitted to Radiotherapy and Oncology
2. T Zhang, Y Chi *et al*, “Automatic Delineation of Online Head-And-Neck Computed Tomography Images: Toward Online Adaptive Radiotherapy”, International Journal of Radiation Oncology, Biology and Physics 2007 68(5): 1572-8.
3. Y Chi, J Liang, T Zhang, *et al*, “Automatic Contour Delineation On Cone Beam CT (CBCT) and Verification”**,** American Association of Physics in Medicine 50th Annual Conference, Huston, TX, 2008 (Abstract).
4. T Zhang, *et al, “Online delineation of head and neck CT images”,* 49th AAPM annual conference, Minneapolis, MN, 2007 (Abstract).
5. D Schulze, T Zhang, *“Techniques of Online IMRT Plan Re-Optimization for Prostate Cancer Treatments”*, 50th ASTRO annual conference, Boston, MA, 2008 (Abstract).

Int. J. Radiation Oncology Biol. Phys., Vol. 68, No. 2, pp. 522–530, 2007

0360-3016/07/$–see front matter

ELSEVIER

doi:10.1016/j.ijrobp.2007.01.038

PHYSICS CONTRIBUTION

AUTOMATIC DELINEATION OF ON-LINE HEAD-AND-NECK COMPUTED TOMOGRAPHY IMAGES: TOWARD ON-LINE ADAPTIVE RADIOTHERAPY

TIEZHI ZHANG, PH.D., YUWEI CHI, PH.D., ELISA MELDOLESI, M.D. AND DI YAN, D.SC.

Department of Radiation Oncology, William Beaumont Hospital, Royal Oak, MI

Purpose: To develop and validate a fully automatic region-of-interest (ROI) delineation method for on-line adaptive radiotherapy.

Methods and Materials: On-line adaptive radiotherapy requires a robust and automatic image segmentation method to delineate ROIs in on-line volumetric images. We have implemented an atlas-based image segmentation method to automatically delineate ROIs of head-and-neck helical computed tomography images. A total of 32 daily computed tomography images from 7 head-and-neck patients were delineated using this automatic image segmentation method. Manually drawn contours on the daily images were used as references in the evaluation of automatically delineated ROIs. Two methods were used in quantitative validation: *(1)* the dice similarity coefficient index, which indicates the overlapping ratio between the manually and automatically delineated ROIs; and *(2)* the distance transformation, which yields the distances between the manually and automatically delineated ROI surfaces.

Results: Automatic segmentation showed agreement with manual contouring. For most ROIs, the dice similarity coefficient indexes were approximately 0.8. Similarly, the distance transformation evaluation results showed that the distances between the manually and automatically delineated ROI surfaces were mostly within 3 mm. The distances between two surfaces had a mean of 1 mm and standard deviation of <2 mm in most ROIs.

Conclusion: With atlas-based image segmentation, it is feasible to automatically delineate ROIs on the head-and-neck helical computed tomography images in on-line adaptive treatments. © **2007 Elsevier Inc.**

Region-of-interest delineation, Deformable image registration, Adaptive radiotherapy, Image-guided radiotherapy.

INTRODUCTION

Dose escalation has been shown to be effective in improving the outcome of cancer radiotherapy (RT) at various sites (1–6). However, collateral damage to normal tissue limits the maximal dose that can be safely delivered (7). RT planning uses computed tomography (CT) images, which represent a snapshot of the anatomic geometry at the time of the treatment planning CT scan. Because of setup variations and anatomic changes, a considerable motion margin must be applied to compensate for patients' anatomic variations. Consequently, a large volume of normal tissue is irradiated by approximately the same radiation intensity as that received by the target. In recent years, image-guided RT (IGRT) has become an important technique in tightening the planning target volume margin (8, 9). On-line imaging modalities, such as ultrasonography, megavoltage CT (10), cone-beam CT (CBCT) on-gantry (11), and CT-on-rail (12), provide on-line volumetric images of the patient during IGRT sessions.

Currently, in IGRT sessions, daily on-line images are registered into planning CT images by rigid-body image registration with six degrees of freedom. Translational position errors may be corrected by shifting the treatment table. Methods have also been proposed to correct or partially correct rotational error by rotating the collimator, the gantry, and/or the table (13–15). However, when the shapes or relative positions of the target and organ-at-risk (OAR) change, simple rigid-body correction techniques may not be sufficient for high-precision RT.

On-line adaptive plan adjustment using daily anatomic geometry and position setup may compensate for target and OAR interfraction variation. A plan adjustment method has been proposed to modify the beam aperture and to deform

Reprint requests to: Tiezhi Zhang, Ph.D., Department of Radiation Oncology, William Beaumont Hospital, 3601 W. Thirteen Mile Rd., Royal Oak, MI 48073. Tel: (248) 551-6583; Fax: (248) 551-3784. E-mail: tiezhi.zhang@beaumont.edu

Conflict of interest: none.

Acknowledgments—We want to thank Dr. Wolfgang Tomé of the University of Wisconsin at Madison and Dr. Todd McNutt of John Hopkins University for helping on the Pinnacle Scripting.

This research was partially supported by the Department of Defense, Prostate Cancer Research Program, under award number W81XWH-07-0083.

Received June 9, 2006, and in revised form Dec 18, 2006. Accepted for publication Jan 16, 2007.

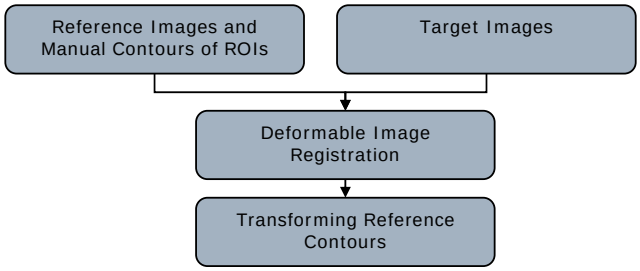

Fig. 1. Flow chart of atlas-based image segmentation. Atlas (reference images with manual contours) was registered to target images. Regions of interests of atlas were mapped to target images subsequently.

fluence map in intensity-modulated RT (16). It might also be possible to reoptimize the intensity-modulated RT plan on-line by using high-performance computing in dose calculation and plan optimization. On-line plan adjustment can, in principle, take account of all setup variation, as well as anatomic geometry changes. It may eventually become a practical form of IGRT.

However, the major obstacle that hinders the clinical implementation of on-line adaptive RT is on-line region-of-interest (ROI) delineation. In three-dimensional treatment planning, ROI contouring is a tedious and time-consuming task for physicians. It is impractical to manually contour all ROIs with the patient on the table. A fast, robust, and automatic ROI delineation method is needed for on-line adaptive treatments.

Atlas-based image segmentation might be a solution for on-line plan adjustments (17–19). Figure 1 shows the procedure of atlas-based image segmentation. An atlas is a reference image data set with previously contoured ROIs. In on-line adaptive RT, the planning CT image and contours are used as the atlas. The planning images are nonrigidly registered to the daily on-line images. ROIs on the planning image are mapped onto daily images using voxel-matching information from deformable image registration. The key component in atlas-based image segmentation is deformable image registration. In this study, we implemented a fast variational-based deformable image registration algorithm (20, 21). The algorithm was used in the atlas-based segmentation of daily head-and-neck (HN) CT images. Automatically delineated ROIs were quantitatively validated through a comparison with manual contours.

METHODS AND MATERIALS

Patient data

A conventional helical CT scanner (Tomoscan SR7000, Philips Medical System, Shelton, CT) was used for image acquisition. Seven HN cancer patients were enrolled in the study. In addition to the treatment planning CT images, 3–6 weekly CT images were acquired for each patient during the RT course. A total of 32 weekly images were acquired from the patients. All images had a slice thickness of 2–3 mm. The resolution was 512 × 512, and the pixel size was 0.973 mm in the transverse plane. Weekly images were used as surrogates of on-line images in the study. Unlike treatment planning CT, no intravenous contrast was administered in the weekly CT acquisitions.

Manual ROI delineation

A commercial treatment planning system (Pinnacle, Philips Medical System, Madison, WI) was used in the contouring of ROIs. A physician manually contoured all ROIs on the planning images, which included the gross tumor volume (GTV), mandible, brainstem, parotids, and lymph nodes. Another physician repeated the contouring on all planning and on-line images independently. Because of the lack of contrast and other medical information, the GTV was not contoured on the on-line images.

All ROIs were dumped into binary ROI masks for data processing. A binary ROI mask M is a three-dimensional matrix with voxels labeled 1 inside and 0 outside the ROI. It is defined as

$$M(\mathbf{x}) = \begin{cases} 1 \Leftrightarrow \mathbf{x} \in O, \\ 0, \ elswhere, \end{cases} \tag{1}$$

where O is a spatial domain that manifests the ROI volume, and $\mathbf{x}$ is a voxel vector.

Deformable image registration

Deformable image registration maximizes the similarity between the reference image R and the floating image T by warping the floating image and, also, keeps the displacement vector fields smooth. A general form of the objective function of grayscale-based deformable image registration is given by the following equation (22):

$$F(\mathbf{u}_f) = D(R, T(\mathbf{u}_f)) + \alpha S(\mathbf{u}_f), \ \alpha > 0 \tag{2}$$

where D is the measure of similarity with respect to the image intensity, S is the smoothness regularizer, $\mathbf{u}_f$ is the displacement vector field, and α is a regulation parameter that controls the relative weights between the two components in the function F.

We chose the sum of the square difference between the two images as the measure of similarity D and the sum of the square gradient of voxel displacement as the smoothness regularizer S, which are defined as

$$D = \int_{x \in \Omega} \|R(\mathbf{x}) - T(\mathbf{x} + \mathbf{u}_f)\|^2 d\mathbf{x}, \tag{3}$$

$$S = \int_{x \in \Omega} \|\frac{\partial \mathbf{u}_f}{\partial \mathbf{x}}\|^2 d\mathbf{x}, \tag{4}$$

where Ω is the domain of the registration. We used a variational-based optimization scheme, in which the local minimum of the objective function was obtained by solving Euler-Lagarange equations (21, 22).

Principally, deformable image registration searches the global minimum of the objective function. Even though locally R and T have different values, the optimization algorithm will still be able to find the best global matching between the images. Thus, the deformable image registration algorithm is applicable to the images with different voxel intensities, such as CT images with and without contrast or helical CT images vs. CBCT images.

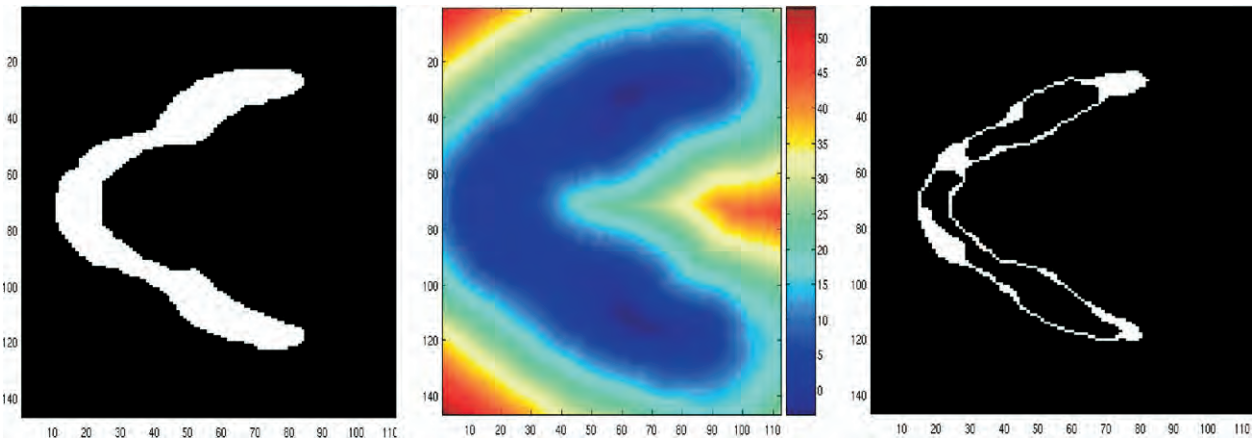

Fig. 2. Evaluation of differences between manually and automatically delineated regions of interest (ROIs) by distance transformation. (Left) Reference (manual) ROI mask; (Middle) distance map of reference ROI mask; and (Right) surface voxels of target (automatic) ROI mask. Nearest distance between manually contoured ROI surface and automatically contoured ROI surface was obtained by overlaying distance maps of reference ROI onto target ROI surface mask.

Multiresolution approaches have been widely used in deformable image registration to alleviate the problem of local minima. We used a multigrid approach to register the image pair with coarse to fine grids at different registration levels (23). As well as maintaining the smoothness of displacement field, the existence of the smoothness regularizer S also limits the range of deformation. The algorithm can be reluctant to match the regions with low contrast and large deformation. To remedy this problem, we reset the displacement fields to zero when registration was completed at each registration level and used the deformed images as new floating images in the next registration level. The displacement fields were saved before resetting.

Automatic image segmentation

Deformable image registration transforms floating images with the displacement map $\mathbf{u}_f$. Thus, we used the planning CT images as floating images and the on-line images as reference images in deformable image registration, so that the displacement map $\mathbf{u}_f$ could be directly used to transform ROI masks on planning images without reversion. The ROI masks on planning images M_p were transformed onto the on-line images according to

$$M_d(\mathbf{x}) = M_p(\mathbf{x} + \mathbf{u}_f), \tag{5}$$

where M_d is the ROI masks on daily on-line images.

We used a Pinnacle Script to generate binary masks of reference ROIs. The reference ROI masks were transformed onto on-line images using displacement maps from deformable image registration. As a consequence, target images were segmented automatically. We used a custom-developed algorithm to convert the ROI masks into Pinnacle's ROI file format so that the ROIs can be displayed in Pinnacle.

Dice similarity coefficient index

The dice similarity coefficient (DSC) index (24) has been widely used in the evaluation of deformable image registration results. In this study, manually contoured ROIs were compared to automatically contoured ROIs using the DSC index. The DSC index is defined as

$$DSC = \frac{2a}{2a + b + c} = \frac{2n\{O_1 \cap O_2\}}{n\{O_1\} + n\{O_2\}} \tag{6}$$

where O_1 is the set of voxels of manual (reference) ROI; O_2 is the set of voxels of automatic (test) ROI; a, representing proper delineation, is the number of voxels common to both data sets; b is the number of voxels unique to O_1; c is the number of voxels unique to O_2; and $n\{\mathrm{O}\}$ is the number of voxels in O. The DSC conformality index approaches 1 when the reference ROI and test ROI overlap exactly.

Distance transformation

A distance map is an image in which the value of each voxel is the distance from the pixel to a given set or object. A Euclidean distance transformation (DT) is an algorithm that computes an Euclidean distance map from a binary image representing this set of voxels (25). In this study, two DTs were performed on the binary masks of manually contoured ROIs. The first DT yielded a distance map with Euclidean voxel distances outside the ROI surfaces. Then, the ROI masks were reversed so that the ROI volumes were labeled with 0 inside and 1 outside. A second DT of the reversed ROI masks yielded the Euclidean voxel distances inside the ROI. The two distance maps were combined with positive distances outside and negative distances inside the ROI. The nearest distances between the reference ROI surfaces and target ROI surfaces were obtained by overlaying the target ROI surface voxels onto the distance matrix of the reference ROI. The distance value at each corresponding surface voxel position was the nearest distance of this surface voxel to the surface of the reference ROI. In this study, the manually contoured ROIs were used as references and the automatically generated ROIs were used as the target ROIs. The DT validation method is shown schematically in Fig. 2.

Three-dimensional DT transformations were performed on binary ROI masks. However, for some ROIs, the ends of the manual contour on the transverse CT slices were not well defined in the images and involved large human variations. To avoid that, the superior end of the brainstem and the inferior end of the spinal cord were masked out in the evaluation.

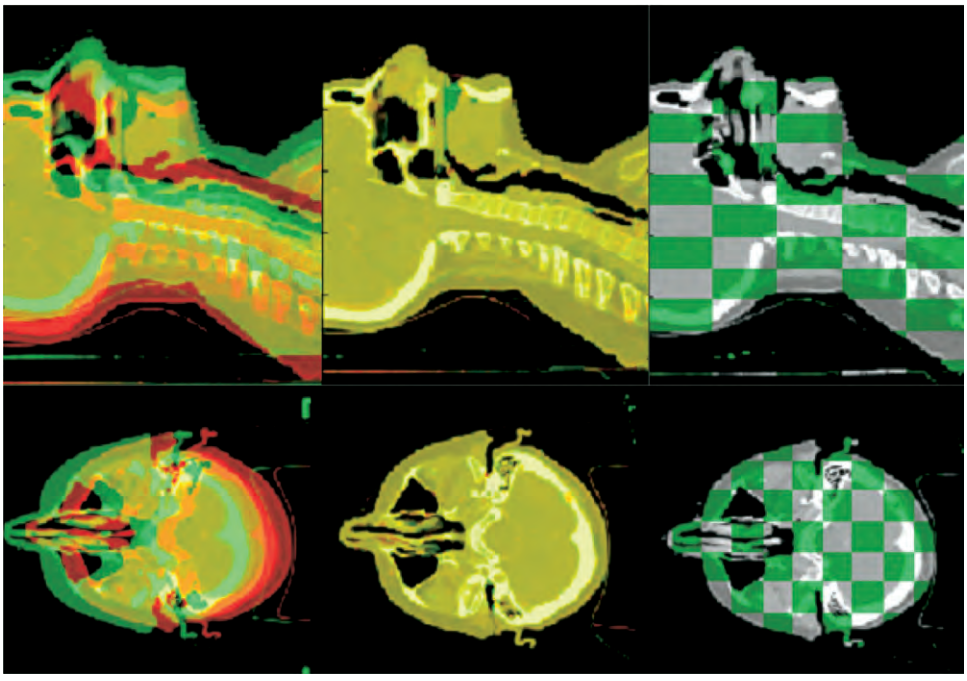

Fig. 3. Deformable image registration of head-and-neck computed tomography images. Images (Left) before and (Middle) after deformable image registration. (Right) Postregistration images by tiled views (gray, reference images; green, floating images).

RESULTS

Deformable image registration

Daily CT images and planning CT images were used as reference images and floating images in deformable image registration, respectively. The results of deformable image registration are shown in Fig. 3. Each image registration process took 10–15 min using a Dell computer workstation with a 3.0-GHz Intel Xeon CPU and 8-G memory. As shown in Fig. 3, the images were different before image registration and highly similar after registration. Minor dis-

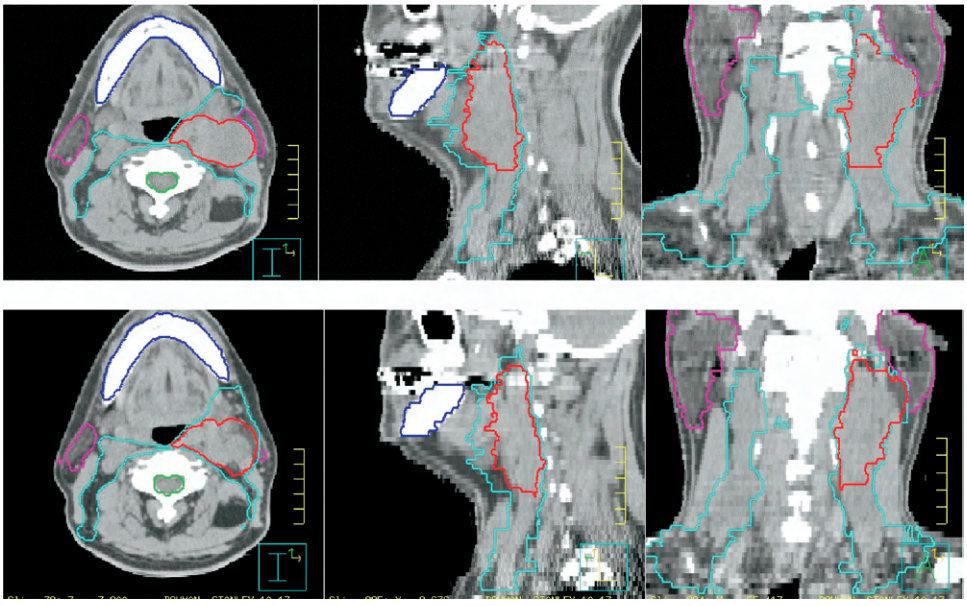

Fig. 4. (Top) Manually drawn contours on planning computed tomography images and (Bottom) automatically delineated regions of interest on on-line images. Contours on on-line images transformed from planning computed tomography images by fully automatic atlas-based image segmentation. Note the consistency of delineation of gross tumor volumes in on-line images. Red indicates gross tumor volume; light blue, nodes; purple, parotid glands; green, spinal cord; and blue, mandible.

crepancies likely stemmed from the intrinsic differences between the image pairs. For example, the dental filling artifacts in the image pairs caused difficulty in registration.

Automatic segmentation

With the deformation information from deformable image registration, the daily images were automatically delineated according to Eq. 5. Figure 4 shows examples of the manually (physician) contoured atlas and automatically contoured on-line images at a treatment day. Qualitatively, the automatically delineated ROIs on on-line images were consistent with manually delineated ROIs on planning images.

Quantitative validation

Another physician also contoured daily CT images. The manually contoured ROIs were used as references. Automatically generated contours were compared with the corresponding manual contours. The discrepancies between the manually and automatically generated contours might have been caused by image registration errors, as well as human variation. Figure 5 shows an example of the three-dimensional surfaces of the manually and automatically delineated ROIs of the same image data set.

The discrepancies between the manual and automatic contours were evaluated with the DSC index. The human-delineated ROIs on the daily images were used as references. The DSC indexes of each ROI in each daily image data set were calculated (Fig. 6).

Discrepancies between the manual and automatic delineation were also measured by DT. Figure 7 shows the histograms of the distances between the manually and automatically contoured ROI surfaces for a typical patient. The distances between the two surfaces were centered close to zero, and the variations were mostly within 2–3 mm. Table 1 lists the mean values and standard deviations of all ROI discrepancies for all patients. The discrepancies between the manual and automatic ROIs all had a mean of 1–3 mm and standard deviation within 2 mm.

Automatic delineation of GTV

Automatic delineation of the GTV is also necessary for on-line adaptive treatment. One major advantage of atlas-based image segmentation is that the boundaries of the ROIs are not necessary located on image features such as the edges. Figure 4 shows the automatically delineated GTVs on the on-line images.

However, manual delineation of targets in HN cancer may not be consistent (26, 27). In some cases, because of its low contrast to surrounding normal tissue, the GTV can be difficult to be delineated on the on-line images without additional information, such as positron emission tomography and magnetic resonance imaging. Moreover, the on-line CT images used in this study were acquired without intravenous contrast. Therefore, the GVT was difficult for the physician to contour with the limited information provided. Thus, automatic segmentation of the GTV was not compared with the manual contours, as was done for the other ROIs in the present study. Physicians visually inspected the GTV contours on the on-line images and accepted the automatic segmentations of the GTV.

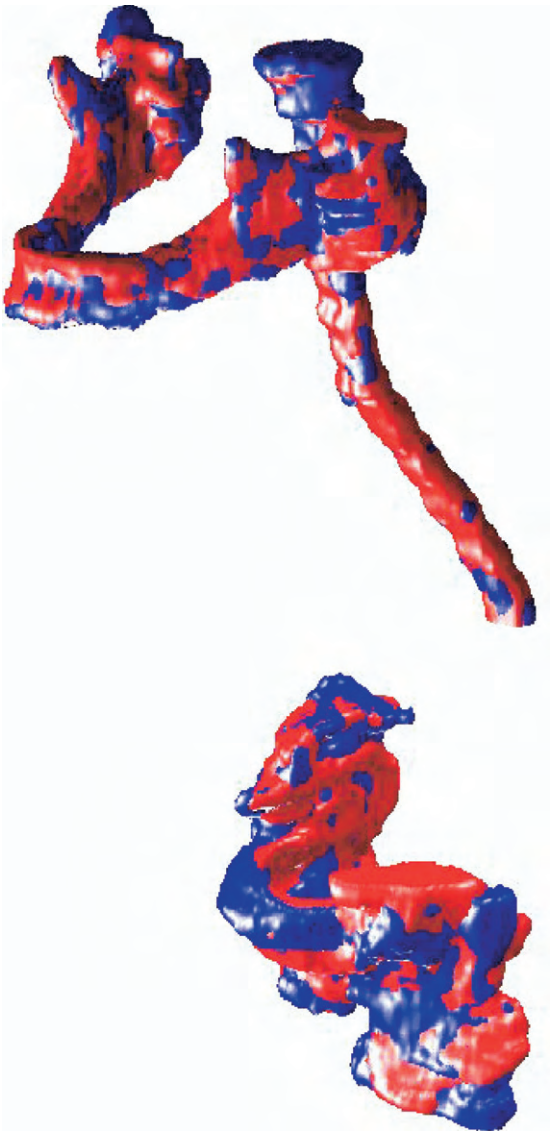

Fig. 5. Three-dimensional surface rending of manual (red) and automatic (blue) regions of interest. (Top) All regions of interest except for nodes. (Bottom) Nodal regions of interest. Overlaid surfaces show overall agreement between regions of interest generated by computer and human.

DISCUSSION

In this study, we implemented and validated an automatic atlas-based image segmentation method to delineate the ROIs of daily HN CT images. Automatic segmentation transforms the contours on planning images into the contours on daily images. Atlas-based image segmentation has many features that are suitable for on-line adaptive treatments. These include

1. Atlas-based image segmentation incorporates *a priori* knowledge about the shape and image characteristics of the ROIs.
2. Atlas-based image segmentation is able to contour the ROI with a boundary that is not located on the edge. The position of contours can be interpolated from surrounding structures.

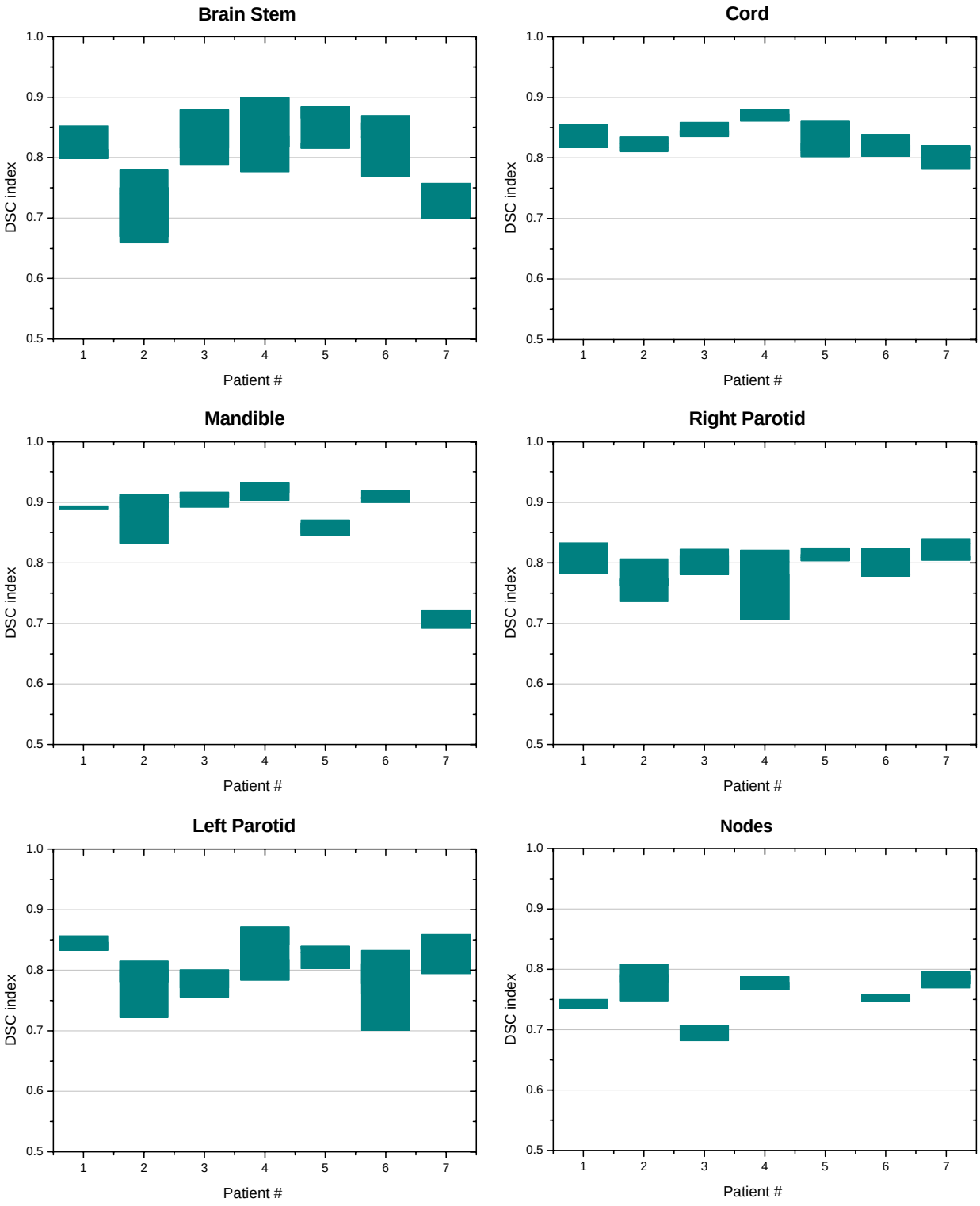

Fig. 6. Dice similarity coefficient (DSC) indexes for automatic region of interest delineations. Manually delineated regions of interests were used as references in evaluation of automatic delineation.

3. Atlas-based image segmentation is able to contour all ROIs at once.

The second feature is crucially important for on-line adaptive treatment. For RT planning, some ROIs do not have significant contrast against the background. Physicians delineate these through the use of previous knowledge of the shape and relative position of the ROIs to more prominent structures. Atlas-based image segmentation mimics the knowledge of the anatomy and radiology experts. It uses *a priori* knowledge about shape and image data

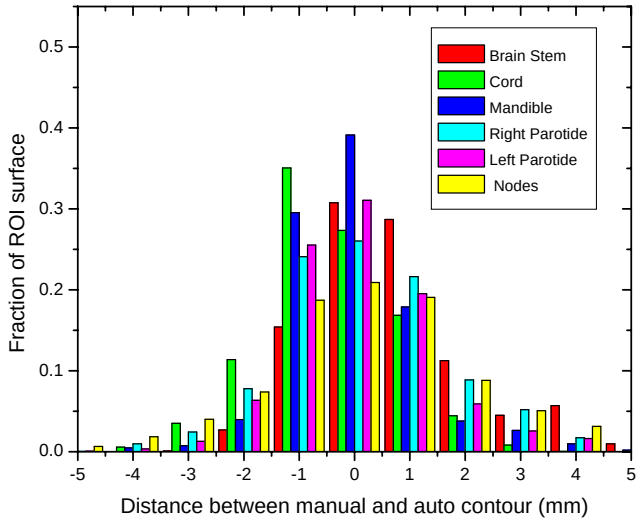

Fig. 7. Histograms of surface distances between manual regions of interest and automatic regions of interest. ROI = regions of interest.

characteristics in the segmentation process. The boundary of some structures, such as the GTV, does not lie on the image edge. Atlas-based image segmentation may interpolate ROI boundaries from nearby structures with more obtrusive contrasts.

Deformable image registration relies on image quality. In the present study, we used CT images from a fan-beam CT scanner. CT-on-rail provides daily helical CT images. Our current automatic ROI delineation method can be directly applied to IGRT by CT-on-rail. Still in its infant stage, CBCT on-gantry is becoming a popular on-line imaging modality for IGRT. The image quality of CBCT is inferior to that of a fan-beam CT scanner. Both scatters and approximate image reconstruction cause significant image artifacts and distortions. More importantly, the signal/noise ratio is dramatically low compared with that of regular fan-beam CT images. Thus, additional improvements may be necessary to make the algorithm immune to the defects of CBCT.

Dental filling artifacts often exist in some HN CT images. Figure 8 shows the automatic segmentation results of HN images with dental filling artifacts. The influence of the artifacts was constrained to a proximate region of a dental filling. Only the mandible contours on a few slices were distorted. Other ROIs were not significantly affected. Many CT reconstruction algorithms have been developed to eliminate or reduce dental filling artifacts. Implementation of these techniques in on-line CT imaging modalities would be beneficial in HN on-line adaptive treatments.

Deformable image registration does not guarantee point-to-point matching. Point-to-point matching is very difficult to validate because the true information is unknown. Previous studies warped the image data set with predetermined displacement fields and then registered the warped image data set back to their original shapes (18, 21). In reality, however, organ shape changes are far more complex than any deformation model can simulate. Fortunately, exact point-to-point matching is unnecessary in on-line re-planning, in which only the ROI boundaries are used. Additional investigations are necessary for off-line adaptive RT, in which point-to-point information is mandatory to obtain accumulated doses.

We validated atlas-based segmentation through a comparison with manual delineation. The discrepancies between the reference manual contours and automatic generated contours included registration errors, as well as human variations. This quantitative validation method is only valid

Table 1. Mean followed by standard deviation of discrepancies between manually and automatically generated contours

Pt. No.	Total images	Brain stem (mm)	Spinal cord (mm)	Mandible (mm)	Right parotid (mm)	Left parotid (mm)	Lymph nodes (mm)
1	3	−0.61	−0.36	−0.08	0.07	0.54	1.72
		1.20	1.07	1.59	1.51	1.76	3.32
2	5	−1.33	0.52	0.07	0.77	2.24	1.62
		2.30	1.25	1.32	2.91	2.72	3.27
3	4	−0.65	0.57	0.04	0.53	1.54	2.35
		1.47	1.07	1.27	1.80	2.62	4.91
4	4	−0.94	0.06	0.10	0.51	0.91	0.96
		1.96	1.22	1.43	1.83	2.02	2.31
5	5	0.40	0.51	−0.02	0.09	0.72	NA*
		2.07	1.14	1.01	1.42	1.79	NA*
6	6	−0.13	0.76	−0.08	1.46	1.81	1.36
		1.63	1.08	1.17	2.28	2.41	2.73
7	5	0.10	0.77	1.09	0.37	0.14	0.82
		1.88	1.08	2.94	1.60	1.75	2.35
All	32	−0.45	0.40	0.16	0.54	1.13	1.47
		1.79	1.13	1.53	1.91	2.15	3.15

Abbreviations: Pt. No. = patient number; NA = not applicable.
* Nodes of Patient 5 were included in gross tumor volume and were not contoured separately.

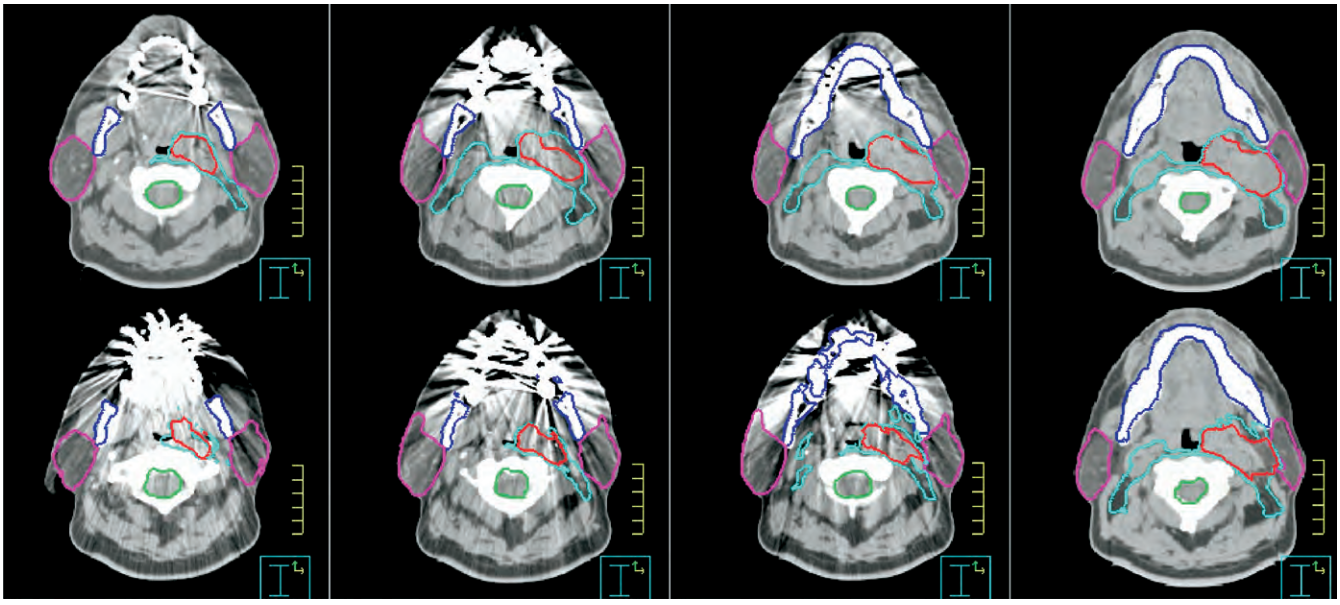

Fig. 8. (Top) Manual and (Bottom) automatic delineations of head-and-neck images with dental filling artifacts. Automatic delineation of mandible in third slice distorted by image artifacts.

when the ROI can be accurately defined by a human, such as has been done for the kidney (28). We have performed repeat manual delineation by two physicians on a few data sets. This limited study showed that all the ROIs, except for the GTV, can be reliably delineated using daily CT images without contrast. Larger scale of studies should be performed to quantify the component of interphysician variations in the overall discrepancies.

Automatic delineation of the GTV is extremely important for on-line adaptive treatment. We have experienced difficulty in the manual delineation of the GTV in daily images without intravenous contrast. As a consequence, automatically generated GTV contours were not quantitatively validated in the same way as the other ROIs in this study. Additional study in GTV validation is necessary for on-line adaptive RT.

CONCLUSION

Atlas-based image segmentation can automatically delineate the ROIs on daily CT images. Quantitative validations demonstrated that this method was robust in contouring ROIs in daily HN fan-beam CT images. Atlas-based image segmentation can be a key component in IGRT by way of on-line replanning, as well as for other on-line adaptive approaches.

REFERENCES

1. Martel MK, Ten Haken RK, Hazuka MB, *et al.* Estimation of tumor control probability model parameters from 3-D dose distributions of non-small cell lung cancer patients. *Lung Cancer* 1999;24:31–37.
2. Grills IS, Yan D, Martinez AA, *et al.* Potential for reduced toxicity and dose escalation in the treatment of inoperable non–small-cell lung cancer: A comparison of intensity-modulated radiation therapy (IMRT), 3D conformal radiation, and elective nodal irradiation. *Int J Radiat Oncol Biol Phys* 2003;57:875–890.
3. Hanks GE, Hanlon AL, Schultheiss TE, *et al.* Dose escalation with 3D conformal treatment: Five year outcomes, treatment optimization, and future directions. *Int J Radiat Oncol Biol Phys* 1998;41:501–510.
4. Kajanti M, Blomqvist C, Lehtonen H, *et al.* Biweekly dose escalation in curative accelerated hyperfractionation for advanced head and neck cancer: A feasibility study. *Int J Radiat Oncol Biol Phys* 1997;39:837–840.
5. Roof KS, Fidias P, Lynch TJ, *et al.* Radiation dose escalation in limited-stage small-cell lung cancer. *Int J Radiat Oncol Biol Phys* 2003;57:701–708.
6. Symon Z, Griffith KA, McLaughlin PW, *et al.* Dose escalation for localized prostate cancer: Substantial benefit observed with 3D conformal therapy. *Int J Radiat Oncol Biol Phys* 2003;57:384–390.
7. Kuban D, Pollack A, Huang E, *et al.* Hazards of dose escalation in prostate cancer radiotherapy. *Int J Radiat Oncol Biol Phys* 2003;57:1260–1268.
8. Mackie TR, Kapatoes J, Ruchala K, *et al.* Image guidance for precise conformal radiotherapy. *Int J Radiat Oncol Biol Phys* 2003;56:89–105.
9. Xing L, Thorndyke B, Schreibmann E, *et al.* Overview of image-guided radiation therapy. *Med Dosim* 2006;31:91–112.
10. Ruchala KJ, Olivera GH, Schloesser EA, *et al.* Megavoltage CT on a tomotherapy system. *Phys Med Biol* 1999;44:2597–2621.
11. Jaffray DA, Siewerdsen JH. Cone-beam computed tomography with a flat-panel imager: Initial performance characterization. *Med Phys* 2000;27:1311–1323.
12. Court L, Rosen I, Mohan R, *et al.* Evaluation of mechanical precision and alignment uncertainties for an integrated CT/LINAC system. *Med Phys* 2003;30:1198–1210.
13. Wu Q, Ivaldi G, Liang J, *et al.* Geometric and dosimetric

evaluations of an online image-guidance strategy for 3D-CRT of prostate cancer. *Int J Radiat Oncol Biol Phys* 2006;64:1596–1609.
14. Yue NJ, Knisely JP, Song H, *et al.* A method to implement full six-degree target shift corrections for rigid body in image-guided radiotherapy. *Med Phys* 2006;33:21–31.
15. Boswell SA, Jeraj R, Ruchala KJ, *et al.* A novel method to correct for pitch and yaw patient setup errors in helical tomotherapy. *Med Phys* 2005;32:1630–1639.
16. Mohan R, Zhang X, Wang H, *et al.* Use of deformed intensity distributions for on-line modification of image-guided IMRT to account for interfractional anatomic changes. *Int J Radiat Oncol Biol Phys* 2005;61:1258–1266.
17. Rohlfing T, Russakoff DB, Maurer CR Jr. Performance-based classifier combination in atlas-based image segmentation using expectation-maximization parameter estimation. *IEEE Trans Med Imaging* 2004;23:983–994.
18. Wang H, Dong L, O'Daniel J, *et al.* Validation of an accelerated "demons" algorithm for deformable image registration in radiation therapy. *Phys Med Biol* 2005;50:2887–2905.
19. Wang H, Dong L, Lii MF, *et al.* Implementation and validation of a three-dimensional deformable registration algorithm for targeted prostate cancer radiotherapy. *Int J Radiat Oncol Biol Phys* 2005;61:725–735.
20. Fischer B, Modersitzki J. Intensity-based image registration with a guaranteed one-to-one point match. *Methods Inf Med* 2004;43:327–330.
21. Lu W, Chen ML, Olivera GH, *et al.* Fast free-form deformable registration via calculus of variations. *Phys Med Biol* 2004; 49:3067–3087.
22. Modersitzki J. Numerical methods for image registration. New York: Oxford University Press; 2003.
23. Kostelec PJ, Weaver JB, Healy DM Jr. Multiresolution elastic image registration. *Med Phys* 1998;25:1593–1604.
24. Bharatha A, Hirose M, Hata N, *et al.* Evaluation of three-dimensional finite element-based deformable registration of pre- and intraoperative prostate imaging. *Med Phys* 2001;28: 2551–2560.
25. Shih FY, Wu YT. The efficient algorithms for achieving Euclidean distance transformation. *IEEE Trans Image Process* 2004;13:1078–1091.
26. Ketting CH, Ustin-Seymour M, Kalet I, *et al.* Consistency of three-dimensional planning target volumes across physicians and institutions. *Int J Radiat Oncol Biol Phys* 1997;37:445–453.
27. Hermans R, Feron M, Bellon E, *et al.* Laryngeal tumor volume measurements determined with CT: A study on intra- and interobserver variability. *Int J Radiat Oncol Biol Phys* 1998; 40:553–557.
28. Rao M, Stough J, Chi YY, *et al.* Comparison of human and automatic segmentations of kidneys from CT images. *Int J Radiat Oncol Biol Phys* 2005;61:954–960.

Comparison of various online IGRT strategies: The benefits of online treatment plan re-optimization

Derek Schulze, M.S., Jian Liang, Ph.D., Di Yan, D.Sc. Tiezhi Zhang, Ph.D.

Department of Radiation Oncology
William Beaumont Hospital, Royal Oak, Michigan, USA.

Corresponding author:
Tiezhi Zhang, PH.D
Radiation Oncology Physics
William Beaumont Hospital
3601 W. Thirteen Mile Rd.
Royal Oak, MI 48073

TEL: (248)551-6583
FAX: (248)551-3784
E-mail: tiezhi.zhang@beaumont.edu

Conflict of Interest Notification

5

None of the authors has any conflicts of interest.

Abstract

Purpose: To compare the dosimetric differences of various online IGRT strategies and predict potential benefits of online re-optimization techniques in prostate cancer radiation treatments.

Material and methods: Nine prostate patients were recruited in this study. Each patient has 1 treatment planning CT images and 10 treatment day CT images. Five different online IGRT strategies were evaluated which include 3D conformal with bone alignment, 3D conformal re-planning via aperture changes, intensity modulated radiation treatment (IMRT) with bone alignment, IMRT with target alignment and IMRT daily re-optimization. Treatment planning and virtual treatment delivery were performed. The delivered doses were obtained using in-house deformable dose mapping software. The results were analyzed using equivalent uniform dose (EUD).

Results: With the same margin, rectum and bladder doses in IMRT plans were about 10% and 5% less than those in CRT plans respectively. Rectum and bladder doses were reduced as much as 20% if motion margin is reduced by 1cm. IMRT is more sensitive to organ motion. Large discrepancies of bladder and rectum doses were observed compared to the actual delivered dose with treatment plan predication. The therapeutic ratio can be improved by 14% and 25% for rectum and bladder respectively if IMRT online re-planning is employed compared to IMRT bone alignment approach. The improvement of target alignment approach is similar with 11% and 21% dose reduction to rectum and bladder respectively. However, undosing in seminal vesicles was observed on certain patients.

Conclusions: Online treatment plan re-optimization may significantly improve therapeutic ratio in prostate cancer treatments. However for low risk patient with only prostate involved, online target alignment IMRT treatment would achieve similar results as online re-planning. For all IGRT

approaches, the delivered organ-at-risk doses may be significantly different from treatment planning prediction.

Introduction

The purpose of treatment-room imaging technologies has been to accurately position the patient for daily treatments. This increased accuracy justifies a smaller clinical target volume to planning target volume (CTV-PTV) margin [1], decreasing the consequent collateral damage to normal tissues. While treatment-room imaging methods are certainly a step forward for radiation oncology, the efficacy of these image-guided treatments depends on a treatment plan optimized using a single snapshot of the patient anatomy, typically via the simulation computed tomography (CT). This planning method assumes that the shape and position of the target do not change from day to day. This assumption is often violated due to setup variation and daily anatomic position changes. As image guidance technologies begin to provide a level of information during each treatment rivaling that available during treatment planning, new strategies should be adopted to ensure that the best treatments are delivered to the greatest number of patients.

Perhaps the key issue in image guidance is how the information is used to modify treatment [2,3]. We classify the online image guided radiation treatments (IGRT) into three different precision levels: (1) *bony alignment,* (2) *target alignment, and* (3) *re-planning.*

Bony alignment: Of the three IGRT strategies, bony alignment has the lowest requirement for online image quality, as projection radiographic image quality allows visibility of high contrast bony landmarks but not soft tissues. This method can be implemented by using electronic portal imaging devices (EPIDs) [4]. In clinical treatment, the 2-D megavoltage (MV) images can be registered to a digitally reconstructed radiograph (DRR) or to treatment planning CT via 2D-3D registration [5]. Depending on the definition of registration volume and image quality, volumetric online images from kilovoltage cone beam CT (kV-CBCT) and MV-CBCT may also be registered at bony structures due

to the high contrast to surrounding soft tissues [6]. Most current IGRT treatments correct only the three translational components of rigid-body motion. Six-degree-of-freedom corrections can be achieved with a robotic couch (Hexpod^{TM}, Medical Intelligence GmbH, Schwabmünchen, Germany) [7] or by rotating the couch, collimator and gantry altogether [8]. In the treatment simulation study, we registered the daily treatment images to the planning CT images at the pelvic bones with six degrees of freedom to simulate bony alignment approach.

Target alignment: Aligning directly to the target requires better image quality. The boundary of the low contrast (soft tissue) treatment target needs to be identified. For prostate treatments in particular, it may be difficult to align the target in IGRT treatment using CBCT due to its inferior image quality. Another approach to align at the target is to use implanted fiducial markers, which are visible through portal imaging [9]. The basic application of this technology would be to identify the target center of mass based on the average position of three markers. In our clinical experience however, we found that the target motion may include large rotational components. It is unrealistic to fully correct the rotation [10]. Thus, in the simulation study, we only correct the translation component by translating to the center-of-mass.

Re-planning: If the target and organs-at-risk (OARs) can be delineated on online volumetric images, it is possible to generate a new plan in each treatment day [11]. For 3D conformal radiation treatment (3D-CRT) plans, the beam aperture can be changed according to the shape of the target seen in the beam's-eye-view (BEV) [12]. For intensity modulated radiation therapy (IMRT) plans, the beamlet weight can be re-optimized on a daily basis to minimize the dose to the OAR while maintaining the target dose [13,14]. It is reasonable to use rectum and bladder walls during inverse planning of prostate cancer treatments, so long as the intra-fraction motion can be limited to a negligible level. With these biologically relevant inverse planning objectives, the dose to the OAR may possibly be

further reduced.

Re-planning theoretically provides the highest precision and does not need specialized hardware such as the robotic couch. However, online re-planning requires superior online image quality, as well as fast and robust algorithms to perform automatic region-of-interest (ROI) delineation [15], dose calculation, and beamlet weight optimization. We are actively developing the techniques to facilitate online re-planning. In this study, we performed both 3D-CRT and IMRT treatment planning and treatment simulation studies for several online IGRT strategies. The purpose of this study is to investigate the potential benefits of the *re-planning* approach in prostate cancer treatments, and to characterize the limits of the other IGRT methods.

Methods and Materials

A. Treatment Planning

Image data from nine prostate cancer patients treated at William Beaumont Hospital in Royal Oak, Michigan were used in this study. The nine patients were randomly selected from our patient database. We assume the magnitude of organ motions of these randomly selected patients represent typical prostate population. Treatment planning CT images were acquired with a conventional helical CT scanner. There was no bowel preparatory instruction or procedure for any simulation or treatment day images. For each of these images, contours of prostate, seminal vesicles (SV), rectum (volume and wall), and bladder (volume and wall) were hand-drawn by a single observer. Based upon the contours, treatment plans were generated using the Pinnacle^{TM} treatment planning system (TPS) (Philips Radiation Oncology System, Madison, Wisconsin). The patients were planned as if they had intermediate or high risk disease, and therefore the CTV included both prostate and seminal vesicles. The average prostate volume was 40.7 cm^3 (range: 22.5 – 54.4 cm^3). OARs were limited to bladder and rectum. The average rectum volume was 120.5 cm^3 (range: 45.0 – 189.5 cm^3).

The prostate shows significant movement relative to the pelvic bones [16]. Thus, a uniform 1-cm CTV-PTV margin is used to compensate for inter-faction organ motion in both 3D-CRT and IMRT treatment plans which are intended for use with the bony alignment treatment method. Results from these treatments will demonstrate the adequacy of a widely practiced IGRT method.

Since the target alignment treatment method can account for translational interfraction motion, the motion margin can be greatly reduced. In the 3D-CRT re-planning and IMRT re-planning methods, all interfraction motions are expected to be compensated, and so there is no motion margin component in the PTV for these methods. This will also give us a feeling about the dosimetric

robustness of various IGRT methods to the target translations, deformations, and rotations involved. Intrafraction motion is neglected in this study.

An arbitrary dose of 91.0 Gy was prescribed to the PTV, though results will focus on relative dose values, scalable to any prescription. All treatment plans used five coplanar beams at 0°, 81°, 144°, 216°, and 279°. DVH-based dose-volume objectives were chosen to minimize bladder and rectum doses while maintaining PTV dose uniformity during inverse planning.

The IGRT approaches and the corresponding treatment planning methods are listed in Table 1. Five 3D-CRT and IMRT treatment planning methods formed the bases for the online IGRT treatments:

1) *CRT 1-cm*: 3D-conformal radiotherapy to 95% of the isocenter with 1-cm CTV-to-PTV margin and 6-mm PTV-to-block penumbra. This plan was used for CRT bony alignment IGRT approach (*CRT bone*).
2) *CRT 0-cm*: 3D-CRT plan to 95% of the isocenter with 0-cm CTV-to-PTV margin and 6- mm PTV-to-block penumbra. This plan was used for CRT re-planning via aperture change approach (*CRT Re-plan*).
3) *IMRT 1-cm:* Inverse-planned IMRT with 1-cm CTV-to-PTV margins and OAR-volume as optimization objectives. This was used for IMRT bone alignment treatments (*IMRT Bone*).
4) *IMRT 0-cm volume*: Inverse-planned IMRT with 0-cm CTV-to-PTV margins and OAR volumes as objectives. This method was used for both IMRT target alignment (*IMRT Target*) and IMRT re-planning with OAR volumes as constraints approach (*IMRT Volume*).
5) *IMRT 0-cm wall:* Inverse-planned IMRT with 0-cm CTV-to-PTV margins and OAR walls in optimization objectives. This method was used for IMRT re-planning with OAR walls as constraints approach (*IMRT Wall*).

B. Virtual Treatment Simulations

In addition to treatment planning CT images, 10 treatment day helical CTs were also acquired for each patient. The treatment day images were acquired during the 6-8 week treatment courses with intervals of 3-5 days. The 10 treatment day images were used to simulate 10 treatment fractions for all online IGRT techniques. The daily images were registered to the planning image using bony anatomy in Pinnacle. The ROIs were manually delineated on all daily images after bony registration. As an indication of the range of interfraction motion, Figure 1 shows a treatment planning image with contours from bone registered daily images overlaid.

Ideally, treating a patient positioned by bony landmarks can be simulated by calculating dose on the daily images. However, due to technical issues with Pinnacle, dose calculation on daily images was not possible for the images where non-zero rotational components exist in registration parameters. Previous studies have shown that replacing a daily CT with the planning CT introduces minimal dose calculation error [17]. Using daily images which were registered to planning image without rotation, we were able to determine that calculating daily dose on the planning image introduces an EUD error in the studied ROIs of less than 1%. Thus in this study, daily treatment dose was calculated using voxel densities from the planning CT, as this method introduces negligible error. Calculating DVHs from dose to daily contours will accurately represent all daily motions, as the rotation present in registered daily images will be preserved in the contour shape.

Retrospective virtual treatment simulations were performed in order to compare different online IGRT treatment methods. Compared to interfraction motion, intra-fraction motion is relatively small [16]. In this study, we only focused on interfraction motion, while intra-fraction motion was neglected. Treatment methods were simulated that were associated with different levels of image guidance. The relationship between planning methods and treatment methods is summarized in Table

1.

Bony alignment: This method can be implemented by using electronic portal imaging devices (EPIDs) [4]. In clinical treatment, the 2-D megavoltage (MV) images can be registered to a digitally reconstructed radiograph (DRR) or to treatment planning CT via 2D-3D registration [5]. Depending on the definition of registration volume and image quality, volumetric online images from kilovoltage cone beam CT (kV-CBCT) and MV-CBCT may also be registered at bony structures due to the high contrast to surrounding soft tissues. As a result, bony alignment has the lowest requirement for online image quality of the three evaluated IGRT strategies. Most current IGRT treatments correct only three translational components of rigid-body motion. Six-degree-of-freedom corrections can be achieved with a robotic couch (Hexpod^{TM}, Medical Intelligence GmbH, Schwabmünchen, Germany) [18] or by rotating the couch, collimator and gantry altogether. Bony alignment was simulated by registering the daily treatment images to the planning CT images at the pelvic bones with six degrees of freedom. Doses for *CRT Bone* and *IMRT Bone* treatments were calculated using the unmodified *CRT 1-cm* and *IMRT 1-cm* plans. This simulates the position correction available from standard imaging systems combined with the robotic couch.

Target alignment: Aligning directly to the target requires better image quality. The boundary of the low contrast (soft tissue) treatment target needs to be identified. For prostate treatments in particular, it may be difficult to align the target in IGRT treatment using CBCT due its inferior image quality. Another approach is to use a portal imager to visualize implanted fiducial markers [9]. One application of this technology that is possible with CBCT would be to identify the target based on the average 3D position of three markers. In our clinical experience however, we found that the target motion may include large rotational components. With the standard couch, it is unrealistic to correct the rotation without modifying the treatment plan. Furthermore, the maximum rotation of the

Hexpod^{TM} robotic couch is about 2.5-3.0 degrees, and so some large rotations cannot be corrected in this fashion. In this study, we simulated an image guided treatment available to many institutions by only translating the isocenter to the daily target's center-of-mass. After moving the isocenter, daily doses were calculated using the original *IMRT 0cm Volume* plans. This approximates the use of implanted markers based upon the assumption that marker position accurately reflects target position. For the purposes of this study, this treatment method was labeled *IMRT Target*.

Re-planning: If the target and organs-at-risk (OARs) can be delineated from online volumetric images, it is possible to generate a new plan in each treatment day. Re-planning with daily anatomy should theoretically be the most optimal IGRT approach available using standard teletherapy delivery technology. However, this method requires superior image quality, as well as fast and robust algorithms to perform automatic region-of-interest (ROI) delineation [15], dose calculation, and treatment plan optimization. We are actively developing the techniques to facilitate online re-planning.

The purpose of this study is to predict the potential benefits of the *re-planning* approach in prostate cancer treatments in comparison to other IGRT methods. With this approach, a new plan was generated from each daily treatment CT image. Conformal and intensity modulated techniques were investigated.

The *CRT Re-plan* treatments started from the *CRT 0-cm* plan. On each treatment day, beam apertures were changed to the daily shape of the target in the beam's-eye view (BEV) [12], but the monitor units (MUs) delivered by each beam were kept the same as in the original treatment plan. This makes the re-planning process much simpler from a computational standpoint, as dose re-calculation is unnecessary.

For intensity modulated radiation therapy (IMRT) plans, the beamlet weight can be re-optimized on a

daily basis to minimize the dose to the OAR while maintaining the target dose [14]. So long as the intra-fraction motion can be limited to a negligible level, it is reasonable to use rectum and bladder walls during inverse planning of prostate cancer treatments,. With these biologically relevant inverse planning objectives, the dose to the OAR may possibly be further reduced.

The *IMRT Re-plan Volume* and *IMRT Re-plan Wall* treatments involve complete re-planning on each treatment day. Moving beyond the *CRT Re-plan* method to these treatments requires overcoming the technical challenges of online dose calculation and beamlet weight optimization. To simulate this process, daily doses were calculated after daily re-planning using the *IMRT 0cm Volume* and *IMRT 0cm Wall* planning methods.

C. Dose accumulation

All daily doses were exported to an in-house dose accumulation software utility [19]. In this utility, a finite element (FE)–based deformable registration algorithm was used to obtain voxel matching information between daily and planning CT images. FE models were created using ROI contours from planning CT images. The daily contours were used as boundary conditions to limit the organ deformation. The deformation state with minimum internal elastic energy was obtained. The voxel displacements were obtained by interpolating the FE results to the CT voxel grid.

With voxel displacements, dose accumulation is straightforward. The accumulated dose *D* at position $\vec{x}$, can be obtained by

$$D(\vec{x}) = \sum_{j=1}^{N} d_j(\vec{x} + \vec{u}), \quad (1)$$

where *N* the total number of fractions, d_j the daily dose from the treatment fraction *j*, and $\vec{u}$ is the daily displacement of the FE sub-volume from its original position $\vec{x}$.

D. Evaluation Methods

Dose from treatment planning and simulated delivery was evaluated using the equivalent uniform dose (EUD), as in Equation 2, where *V* is the reference volume, and *D(v)* is the dose to the sub-volume *v*.

$$EUD(V,a) = \left(\sum_{v \in V} \frac{v}{V} \cdot D^{a}(v) \right)^{1/a} \quad (2)$$

As in previous studies [20], the volume parameter for prostate and seminal vesicles was chosen as a= -7. With regard to normal tissues, values were chosen as a=2 for bladder, and a=8.33 for rectum.

Results

A. Comparisons of treatment planning results:

This study included five different treatment planning methods. 3D-CRT and IMRT were used in treatment planning and different treatment planning methods used different CTV-PTV margins (0-cm and 1-cm). The EUDs of the OARs (rectum and bladder) were calculated and compared to the prostate EUD. Unless otherwise noted, percentage values discussed in the following treatment results are based upon the target (prostate) EUD dose in the respective treatment plan.

In order to provide a complete description of results from one randomly selected patient, Figure 2 shows the dose-volume histograms (DVHs) of one patient (#9) from the five planning methods studied. It can be seen that IMRT plans have less homogeneous target dose. Bladder dose appears to be similar for both plans with 1cm margins. IMRT significantly reduces rectum dose. Rectum dose is similar for the *CRT 0cm* method and *IMRT 1cm* method even though the later one has 1cm interfraction margin.

The planned bladder and rectum EUDs for all patients are summarized in Table 2. For the same patient, OAR doses by all treatment planning methods were also normalized to *IMRT 1-cm* plan. When rectum and bladder walls were used in IMRT optimization, the shapes of the dose distributions look different as compared to using the volumes. The top panels of Figure 3 show the fluence maps of the anterior-posterior (AP) beam and isodose distributions from *IMRT 0cm Volume* and *IMRT 0cm Wall* plans. In the volume-based plan, fluence is decreasing where the beam passes a greater distance through the whole organ, while intensity in the wall-based plan is decreased only in a ring where pathlength through the bladder wall is greater. The isodose lines form a “W” shape as they first

retract along the walls, then extend into the center of bladder and rectum in *IMRT Wall* plan. On the contrary, the *IMRT Volume* plan has lower weightings for the beamlets through the center of the bladder, with isodose lines extending a minimum distance into any part of the sensitive organs. Despite this obvious qualitative difference, the improvement of the bladder and rectum EUD dose (as a percent of prostate dose) from *IMRT Volume* to *IMRT Wall* plans is barely noticeable at 1.01 +/- 0.97% and 1.71 +/- 1.53%, respectively.

Selecting an altogether different planning method has a greater impact on the OAR dose than changing the particular definition of the normal tissue volume. With the same 0-cm margin, IMRT plans (*IMRT Volume* and *IMRT Wall*) reduced bladder dose by an average of only 3% compared to 3D-CRT plans (CRT-0-cm), and rectum doses were reduced by 11%. When using a 1-cm margin, there are decreases when changing from CRT to IMRT plans in rectum and bladder doses, by about 7% and 6% of target dose, respectively. The choice of an appropriate CTV-PTV margin is a more important factor that determines OAR doses. For the same planning method, the rectum dose in 0-cm margin plans is respectively 10% and 11% lower using CRT and IMRT methods than their corresponding plans with 1-cm margins. The bladder dose reductions are even larger, at 15% and 14% when a 0-cm margin is used instead of a 1-cm margin for CRT and IMRT respectively.

B. Virtual treatment simulation results:

Fractional dose: The fractional doses for different online IGRT strategies were calculated using the methods described in previous sections. Histograms of differences of the individual fraction dose from the planned EUD can be seen in Figure 4 for all treatment fractions (N=90). All IGRT strategies were able to deliver consistent dose to the prostate. However, dose to seminal vesicle (as a fraction of planned seminal vesicle dose) was reduced by more than 20% in one fraction from the *IMRT Target* method. On this day, the prostate had moved 0.17cm to the posterior from the planning position while the seminal vesicles had moved 1.35cm in the anterior direction. There were several fractions where *IMRT Bone* delivered a seminal vesicle dose that was at least 5% less than planned. Bladder dose deviation appears to be similarly random for all treatment methods. In the rectum, only the two 3D-CRT methods delivered dose that was consistently within ±10% of the planned amount. But remember rectum dose is much higher in CRT plan than IMRT plan.

Accumulated dose: The fractional doses were accumulated using in-house FE-based dose accumulation software. Figure 5 shows the DVH of accumulated dose for Patient #9. Figure 6 shows the accumulated doses for all patients after ten fractions. The EUD values were normalized to the target (prostate) EUD in the treatment plan of the same patient with the same IGRT strategy. The prostates were all well covered, with only one patient's EUD value at about 97% in the IMRT target alignment approach. Seminal vesicles, however, showed a larger difference, with the IMRT target alignment approach showing more severe underdose than other methods. The delivered EUD was only about 93% of the planned value on patient #2. Even with 1-cm CTV-PTV margin, the IMRT bone-alignment showed slight underdose on patients #2 and #9. The accumulated dose results support the conclusion derived from individual fraction doses, that IMRT is more sensitive to organ motion

than 3D-CRT treatments.

Table 3 summarizes rectum and bladder doses achieved by different online IGRT approaches. Remarkable differences in OAR doses are observed when choosing different online IGRT strategies. The *CRT Bone* approach delivered the highest OAR doses, with the bladder and rectum respectively on the average receiving 91% and 71% of target dose. IMRT re-planning approaches obtained the lowest bladder and rectum doses, with average values of 68-69% of target dose to rectum and 49-50% to the bladder. The IMRT target alignment approach obtained OAR doses that are similar to though slightly (1-5%) higher than the IMRT re-planning approaches on most patients. It should be noted that even though the IMRT target alignment method results in similarly low OAR dose, it did not deliver as reliable seminal vesicle dose as re-planning approaches. However, if only prostate is the target, IMRT target alignment method would be close to re-planning approach.

Difference from treatment plan prediction: A major purpose of treatment planning is to predict OAR doses. With an estimate of the risk of complication based on this dose, an appropriate maximum prescription dose can be determined. However, due to the organ motion, the actual delivered dose may be very different from the prediction in the treatment plan. We plotted the discrepancies between treatment plan prediction and accumulated dose after virtually simulated delivery in Figure 7. For all IGRT approaches, the deviation of prostate dose is small. Online IMRT re-planning approaches show small but noticeable target dose variations. This is due to the daily geometry changes that altered the weightings of optimization components. Thus, it may be necessary to re-scale the monitor units (MUs) based on the prostate dose in daily re-optimization. The seminal vesicles show large variations from IMRT bone and target localization approaches.

The rectum doses show large plan-delivery discrepancies in all IMRT treatments. Although the mean discrepancy across all patients is close to zero, the standard deviation is larger than 5%. The standard

deviation is slightly smaller in IMRT re-planning approaches, but not very significant. The 3D-CRT treatments are more consistent, as the mean of discrepancies is close to zero and standard deviation is smaller than 3%. For bladder, all online IGRT approaches show large variations from treatment plan predictions. The standard deviation of plan-delivery discrepancies is large, around 15% in most IGRT approaches, while the standard deviations for IMRT re-planning approaches are smaller, at about 10%.

Discussion

The challenge of radiation therapy has always been to deliver the maximum dose to the target without destroying normal tissues. This has been achievable by strategically treating volumes greater than the clinical target tissues to the prescription dose in order to achieve a high probability of treatment success in spite of daily tumor position uncertainty. Many studies have been done to typify organ motion, and a number of CTV-to-PTV margin recipes [21,22] have been devised to make the selection of margin size a more informed decision. Schaly [2] found that normal tissue dose is not reduced with image guidance alone, but by with the combination of image guidance with smaller CTV-PTV margins. One goal of this study is to demonstrate the extent to which online adaptive image guidance can replace the motion margin.

Interfraction motion has been recognized as the largest contributor to target position uncertainty in tumors unaffected by respiratory motion [16]. In this study, intrafraction motion was not simulated. Ghilezan *et al* showed that prostate intrafraction motion correlated with rectal filling [20] and the amplitude of motion increased with elapsed time. This suggested the importance of shortening treatment time. Recently study by Nijkamp *et al* show that the diet and laxatives can reduce prostate motion during treatment [23]. The patients in this study had no special procedures to limit rectal filling, so our results represent an upper limit of therapeutic ratio which may be lower for patients who do use methods to control rectal volume. Also, a realistic margin would compensate for other uncertainties, such as errors in contouring, image registration, and position alignment.

Technologies such as EPIDs, CALYPSO, CBCT, and CT-on-rails allow accurate tracking of the target on a daily basis, and their use justifies reduction of the margin size. With no margins, the *IMRT Target* simulations essentially treated only the CTV. While there was underdosing in the

seminal vesicles, satisfactory prostate dose was achieved for most patients. This result indicates that much smaller margins are justified around the prostate than the seminal vesicles, and that when treating prostate alone by this method, the size of the motion margin can be dictated only by the extent of intra-fraction motion. For low risk patients, using implanted markers to locate the target each day can significantly reduce normal tissue dose while maintaining target coverage. For patients with high risk disease, the chance of microscopic or occult disease is increased. In the case of prostate patients, this is evidenced by extracapsular extension [24] and seminal vesicle involvement [25]. While the CTV-PTV margin has nominally accounted for target motion, its unintentional function has been to also treat these cells that are not traditionally included in the CTV. Therefore, this extremely conformal approach, which does not account for target rotations and deformations, is expected to be less successful in high risk patients.

Increasing levels of image guidance complexity provide more information with which to re-evaluate the treatment on a more frequent basis. The *CRT Re-plan* method using aperture change makes easy use of this information, as it simply shapes the blocks each day to the new PTV. After ten treatment fractions, the rectum dose from this method was very similar to that from the more standard *IMRT Bone* method. Also, Figure 7 shows that all patients received adequate seminal vesicle dose and 8 of 9 patients received lower bladder dose by the CRT re-planning method. Though normal tissue sparing is limited by the convexity of the dose distribution and the penumbra size, this treatment provides very consistent target coverage. In reality, this treatment is not feasible in the absence of robust automatic contouring technology. However, since this method requires no further optimization, it is probably the least computationally intensive online adaptation that can be performed with this image data.

The most computationally intensive adaptation would involve a complete IMRT re-optimization of

the original treatment plan. Compared to the *IMRT Bone* treatments, target coverage was maintained for all patients while bladder and rectum doses were respectively reduced by approximately 16% and 11%. This approach requires online ROI delineation and online plan re-optimization techniques. Although challenging, it is feasible to achieve these goals in the near future. We have developed an automatic ROI delineation method for HN images [15]. In principle, the same method can also be used on prostate images, but CBCT image quality is a major obstacle. In order to perform IMRT re-planning *online*, high performance computing techniques can be employed to accelerate computation. We were able to accelerate the deformable image registration speed by a factor close to the number of processing elements using a Beowulf cluster. Wu showed that online IMRT re-optimization and MLC leaf conversion are achievable within 2-3 minutes [13].

In this study, we employed online IMRT re-planning approaches in which bladder and rectum volumes or walls were used as optimization constraints. The resulting difference between the two approaches, *IMRT Re-plan Volume* and *IMRT Re-plan Wall*, was shown to be small. When choosing OAR walls instead of the standard volumes, reduction of doses to bladder and rectum is limited to less than 1% on average, though using this approach does not drastically increase technical complexity. Extracting bladder and rectum walls from volumes would be straightforward, so it would be reasonable to employ the IMRT-wall approach for a small but cost-free improvement. This conclusion applies specifically to online re-planning methods, as any benefit from standard planning methods is expected to be negated by interfractional tissue shape changes.

An interesting result of this study is that IMRT techniques are much more sensitive to organ motion than CRT techniques. This is because the IMRT plan is more conformal, meaning that the dose gradient surrounds the target more tightly. Even with a 1-cm margin, underdoses in SV were still observed in several patients. Thus, regardless of margin size, high precision image guidance is more

important in highly conformal treatment techniques. From this result, we would expect image guidance to be a decisive factor in proton prostate cancer treatments, where sharp dose gradients beyond the Bragg peak combined with particle penetration depth uncertainties create opportunities for significant dosimetric consequences.

We noticed that even in the online re-planning techniques, large discrepancies are shown between planning and accumulated bladder and rectum doses. This encourages an close-loop adaptive treatment technique with dose tracking, in which the re-planning takes account of accumulated dose up to that point in the treatment course [26,27]. Otherwise, OAR doses meet constraints in treatment planning, they are likely over the limits in actual treatments.

Conclusions

Online treatment plan re-optimization may significantly improve therapeutic ratio in prostate cancer treatments. However for low risk patient with only prostate involved, online target alignment IMRT treatment would achieve similar results as online re-planning. For all IGRT approaches, the delivered organ-at-risk doses may be significantly different from treatment planning prediction.

Acknowledgements

This study is partially supported by department of defense prostate cancer research program under award #W81XWH-07-0083.

Reference List

1. Beltran C, Herman MG, and Davis BJ. Planning target margin calculations for prostate radiotherapy based on intrafraction and interfraction motion using four localization methods. *Int.J.Radiat.Oncol.Biol.Phys.* 2008;70:289-295.

2. Schaly B, Bauman GS, Song W, Battista JJ, and Van DJ. Dosimetric impact of image-guided 3D conformal radiation therapy of prostate cancer. *Phys.Med.Biol.* 2005;50:3083-3101.

3. Ling CC, Yorke E, and Fuks Z. From IMRT to IGRT: frontierland or neverland? *Radiother.Oncol.* 2006;78:119-122.

4. Herman MG. Clinical use of electronic portal imaging. *Semin.Radiat.Oncol.* 2005;15:157-167.

5. Jans HS, Syme AM, Rathee S, and Fallone BG. 3D interfractional patient position verification using 2D-3D registration of orthogonal images. *Med.Phys.* 2006;33:1420-1439.

6. Stutzel J, Oelfke U, and Nill S. A quantitative image quality comparison of four different image guided radiotherapy devices. *Radiother.Oncol.* 2008;86:20-24.

7. Guckenberger M, Meyer J, Wilbert J, Baier K, Sauer O, and Flentje M. Precision of image-guided radiotherapy (IGRT) in six degrees of freedom and limitations in clinical practice. *Strahlenther.Onkol.* 2007;183:307-313.

8. Yue NJ, Knisely JP, Song H, and Nath R. A method to implement full six-degree target shift corrections for rigid body in image-guided radiotherapy. *Med.Phys.* 2006;33:21-31.

9. Chung PW, Haycocks T, Brown T, Cambridge Z, Kelly V, Alasti H, Jaffray DA, and Catton CN. On-line aSi portal imaging of implanted fiducial markers for the reduction of interfraction error during conformal radiotherapy of prostate carcinoma. *Int.J.Radiat.Oncol.Biol.Phys.* 2004;60:329-334.

10. Wertz H, Lohr F, Dobler B, Mai S, Welzel G, Boda-Heggemann J, and Wenz F. Dosimetric consequences of a translational isocenter correction based on image guidance for intensity modulated radiotherapy (IMRT) of the prostate. *Phys.Med.Biol.* 2007;52:5655-5665.

11. Ding GX, Duggan DM, Coffey CW, Deeley M, Hallahan DE, Cmelak A, and Malcolm A. A study on adaptive IMRT treatment planning using kV cone-beam CT. *Radiother.Oncol.* 2007;85:116-125.

12. Feng Y, Castro-Pareja C, Shekhar R, and Yu C. Direct aperture deformation: an interfraction image guidance strategy. *Med.Phys.* 2006;33:4490-4498.

13. Wu QJ, Thongphiew D, Wang Z, Mathayomchan B, Chankong V, Yoo S, Lee WR, and Yin

FF. On-line re-optimization of prostate IMRT plans for adaptive radiation therapy. *Phys.Med.Biol.* 2008;53:673-691.

14. Wu C, Jeraj R, Olivera GH, and Mackie TR. Re-optimization in adaptive radiotherapy. *Phys.Med.Biol.* 2002;47:3181-3195.

15. Zhang T, Chi Y, Meldolesi E, and Yan D. Automatic delineation of on-line head-and-neck computed tomography images: toward on-line adaptive radiotherapy. *Int.J.Radiat.Oncol.Biol.Phys.* 2007;68:522-530.

16. Langen KM and Jones DT. Organ motion and its management. *Int.J.Radiat.Oncol.Biol.Phys.* 2001;50:265-278.

17. Orton NP and Tome WA. The impact of daily shifts on prostate IMRT dose distributions. *Med.Phys.* 2004;31:2845-2848.

18. Guckenberger M, Meyer J, Wilbert J, Baier K, Sauer O, and Flentje M. Precision of image-guided radiotherapy (IGRT) in six degrees of freedom and limitations in clinical practice. *Strahlenther.Onkol.* 2007;183:307-313.

19. Yan D, Jaffray DA, and Wong JW. A model to accumulate fractionated dose in a deforming organ. *Int.J.Radiat.Oncol.Biol.Phys.* 1999;44:665-675.

20. Ghilezan M, Yan D, Liang J, Jaffray D, Wong J, and Martinez A. Online image-guided intensity-modulated radiotherapy for prostate cancer: How much improvement can we expect? A theoretical assessment of clinical benefits and potential dose escalation by improving precision and accuracy of radiation delivery. *Int.J.Radiat.Oncol.Biol.Phys.* 2004;60:1602-1610.

21. Beltran C, Herman MG, and Davis BJ. Planning Target Margin Calculations for Prostate Radiotherapy Based on Intrafraction and Interfraction Motion Using Four Localization Methods. *Int.J.Radiat.Oncol.Biol.Phys.* 2007.

22. van Herk M, Remeijer P, and Lebesque JV. Inclusion of geometric uncertainties in treatment plan evaluation. *Int.J.Radiat.Oncol.Biol.Phys.* 2002;52:1407-1422.

23. Nijkamp J, Pos FJ, Nuver TT, de JR, Remeijer P, Sonke JJ, and Lebesque JV. Adaptive radiotherapy for prostate cancer using kilovoltage cone-beam computed tomography: first clinical results. *Int.J.Radiat.Oncol.Biol.Phys.* 2008;70:75-82.

24. Chao KK, Goldstein NS, Yan D, Vargas CE, Ghilezan MI, Korman HJ, Kernen KM, Hollander JB, Gonzalez JA, Martinez AA, Vicini FA, and Kestin LL. Clinicopathologic analysis of extracapsular extension in prostate cancer: should the clinical target volume be expanded posterolaterally to account for microscopic extension? *Int.J.Radiat.Oncol.Biol.Phys.* 2006;65:999-1007.

25. Kestin L, Goldstein N, Vicini F, Yan D, Korman H, and Martinez A. Treatment of prostate cancer with radiotherapy: should the entire seminal vesicles be included in the clinical target

volume? *Int.J.Radiat.Oncol.Biol.Phys.* 2002;54:686-697.

26. Birkner M, Yan D, Alber M, Liang J, and Nusslin F. Adapting inverse planning to patient and organ geometrical variation: algorithm and implementation. *Med.Phys.* 2003;30:2822-2831.

27. Wu Q, Liang J, and Yan D. Application of dose compensation in image-guided radiotherapy of prostate cancer. *Phys.Med.Biol.* 2006;51:1405-1419.

Table 1

Planning Method	CTV-PTV Margin	Organs at Risk	Image Guidance	Treatment Name
CRT 1cm	1 cm	n/a	Bony Alignment	*CRT Bone*
CRT 0cm	0 cm	n/a	Block shaped to daily PTV	*CRT Re-plan*
IMRT 1cm	1 cm	bladder & rectum volumes	Bony Alignment	*IMRT Bone*
IMRT 0cm volume	0 cm	bladder & rectum volumes	Isocenter shifted to daily PTV center of mass	*IMRT Target*
IMRT 0cm volume	0 cm	bladder & rectum volumes	Complete daily IMRT re-optimization	*IMRT Re-plan Volume*
IMRT 0cm wall	0 cm	bladder & rectum walls	Complete daily IMRT re-optimization	*IMRT Re-plan Wall*

Table 1. A summary of IGRT approaches simulated in this study. The information of a row from left to right describes how a planning method relates to an IGRT treatment method.

Table 2

Rectum

Patient #	CRT 1-cm	CRT 0-cm	IMRT 1-cm	IMRT volume	IMRT wall
1	95.0%	84.3%	82.3%	67.8%	66.7%
2	88.9%	82.5%	85.9%	74.4%	75.4%
3	88.5%	80.5%	88.1%	74.1%	70.2%
4	92.5%	84.6%	82.9%	77.4%	74.2%
5	89.9%	80.3%	82.1%	72.6%	70.7%
6	93.6%	83.6%	83.3%	70.7%	70.1%
7	89.4%	77.9%	85.2%	70.2%	68.4%
8	92.3%	80.1%	85.7%	71.1%	68.0%
9	94.7%	84.6%	82.8%	72.0%	71.2%
Mean	91.6%	82.1%	84.3%	72.3%	70.5%

Bladder

Patient #	CRT 1-cm	CRT 0-cm	IMRT 1-cm	IMRT volume	IMRT wall
1	78.6%	63.6%	67.7%	56.2%	54.0%
2	76.2%	59.6%	67.3%	52.4%	52.8%
3	50.9%	40.1%	52.5%	40.8%	39.7%
4	63.3%	49.4%	58.1%	48.1%	48.3%
5	70.5%	53.0%	64.7%	51.6%	50.3%
6	83.5%	66.8%	73.2%	59.5%	57.4%
7	60.8%	47.3%	58.7%	47.5%	45.8%
8	64.9%	48.3%	60.0%	46.9%	45.7%
9	59.3%	45.9%	56.4%	45.0%	44.9%
Mean	67.6%	52.7%	62.1%	49.8%	48.8%

Table 2: Comparison of planned rectum and bladder EUD doses from various treatment planning methods. The values are expressed as percentages of target (prostate) EUD dose.

Table 3

Rectum

Patient #	CRT Bone	CRT Re-plan	IMRT Bone	IMRT Target	IMRT Re-plan Volume	IMRT Re-plan Wall
1	94.5%	83.3%	85.2%	73.4%	68.3%	67.8%
2	87.4%	80.8%	72.0%	63.6%	65.9%	66.4%
3	85.7%	80.8%	73.1%	75.4%	69.4%	66.3%
4	92.1%	81.9%	80.2%	70.1%	70.7%	70.1%
5	89.8%	79.7%	82.9%	72.6%	69.4%	68.2%
6	92.4%	83.6%	84.0%	72.7%	71.8%	71.8%
7	88.9%	78.8%	77.6%	68.6%	65.0%	64.2%
8	90.2%	79.1%	83.2%	73.3%	70.1%	69.3%
9	93.5%	81.8%	78.4%	70.6%	70.1%	68.4%
Mean	90.5%	81.1%	79.6%	71.1%	69.0%	68.0%

Bladder

Patient #	CRT Bone	CRT Re-plan	IMRT Bone	IMRT Target	IMRT Re-plan Volume	IMRT Re-plan Wall
1	75.5%	66.4%	61.9%	56.8%	55.7%	54.9%
2	81.5%	61.3%	71.8%	53.5%	51.8%	51.7%
3	68.9%	48.7%	69.7%	51.8%	48.3%	47.6%
4	76.9%	54.1%	68.1%	55.9%	50.5%	50.3%
5	74.5%	56.7%	69.5%	57.2%	53.1%	52.4%
6	81.8%	66.8%	74.1%	60.6%	61.5%	60.0%
7	60.3%	41.5%	58.6%	42.4%	41.7%	40.5%
8	62.7%	41.7%	58.3%	41.4%	42.1%	40.8%
9	60.2%	46.0%	57.7%	45.5%	44.9%	44.3%
Mean	71.3%	53.7%	65.5%	51.7%	49.9%	49.2%

Table 3: Comparison of delivered rectum and bladder doses by different online IGRT methods. The values are expressed as percentages of target (prostate) dose.

Figure 1

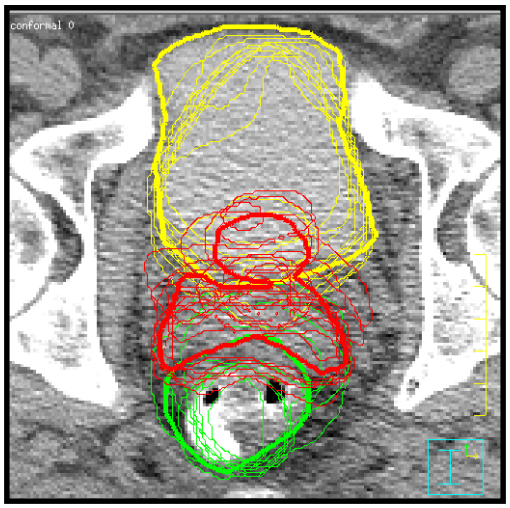

Figure 1. Planning CT showing bladder (yellow), CTV (red), and rectum (green) contours. Thick lines define contours from the planning day. Thin lines show the positions of the organs on different treatment days. Contours were generated after registration of bony anatomy.

Figure 2

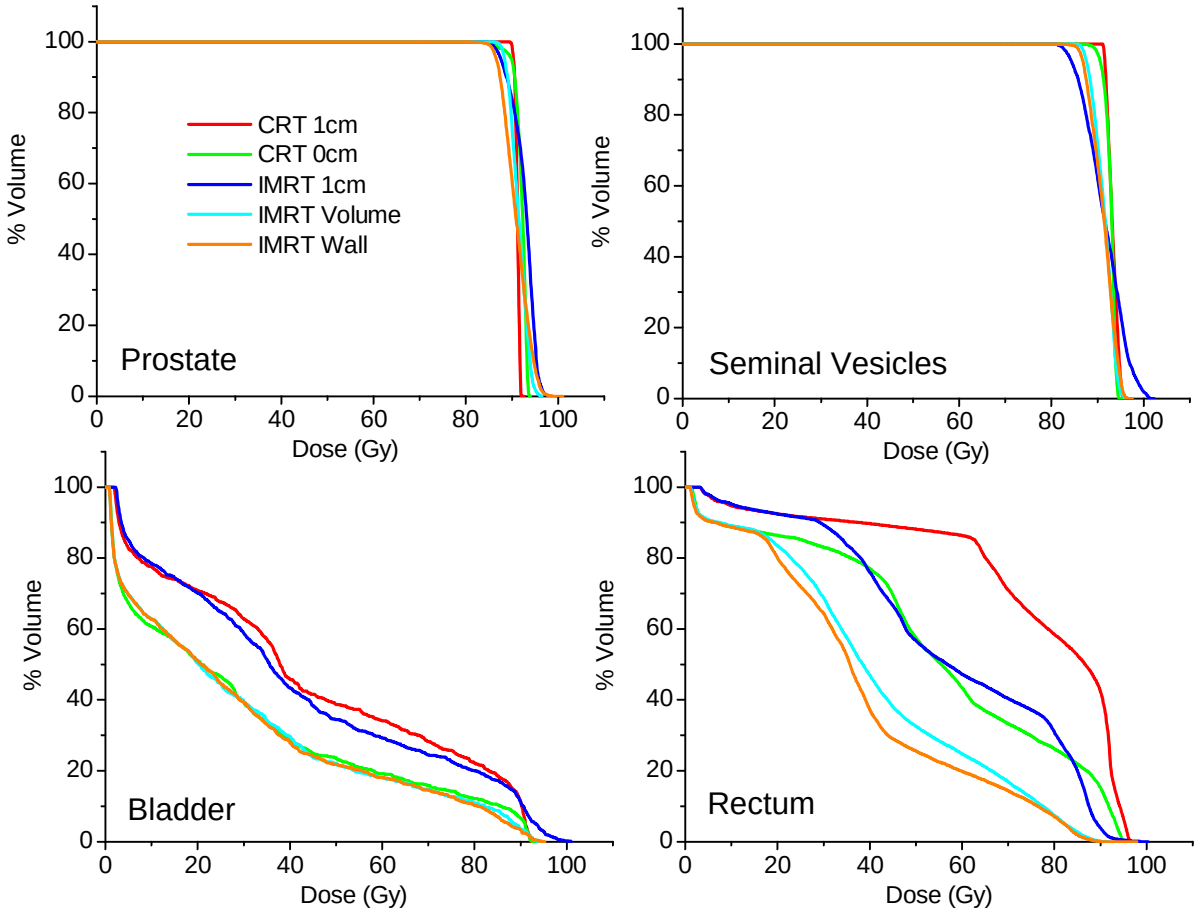

Figure 2 Comparison of dose from five treatment planning methods for Patient #9, described by dose-volume histograms.

Figure 3

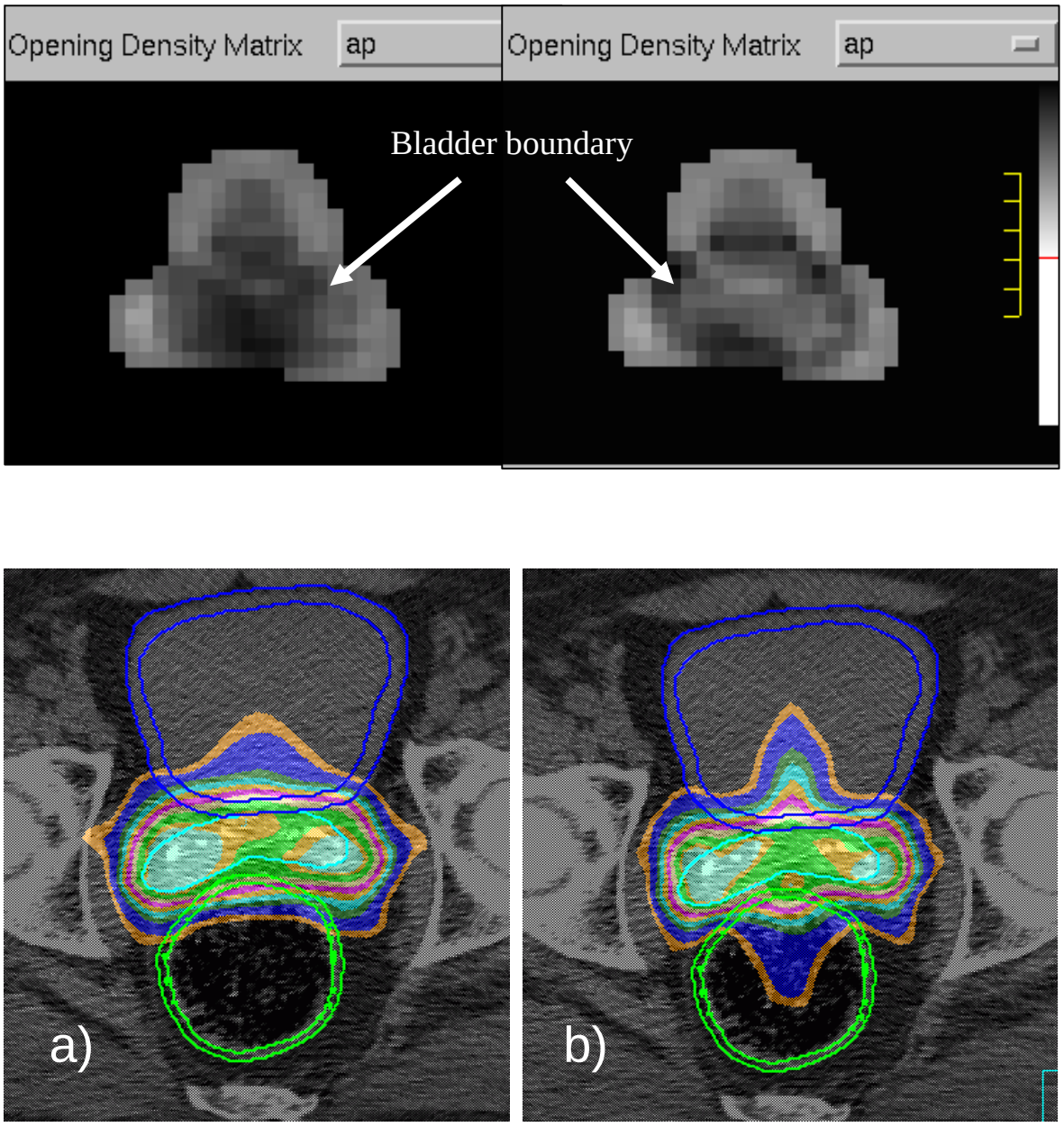

Figure 3. Top: AP beam fluences from treatment plans optimized with OAR volume (left) and OAR wall (right). Bottom: Isodose profiles from IMRT treatment plans using a) organ volumes and b) organ walls. Bladder wall, seminal vesicles, and rectum wall are contoured in dark blue, light blue, and green, respectively. Isodose levels range from 55-105% of the isocenter dose.

Figure 4

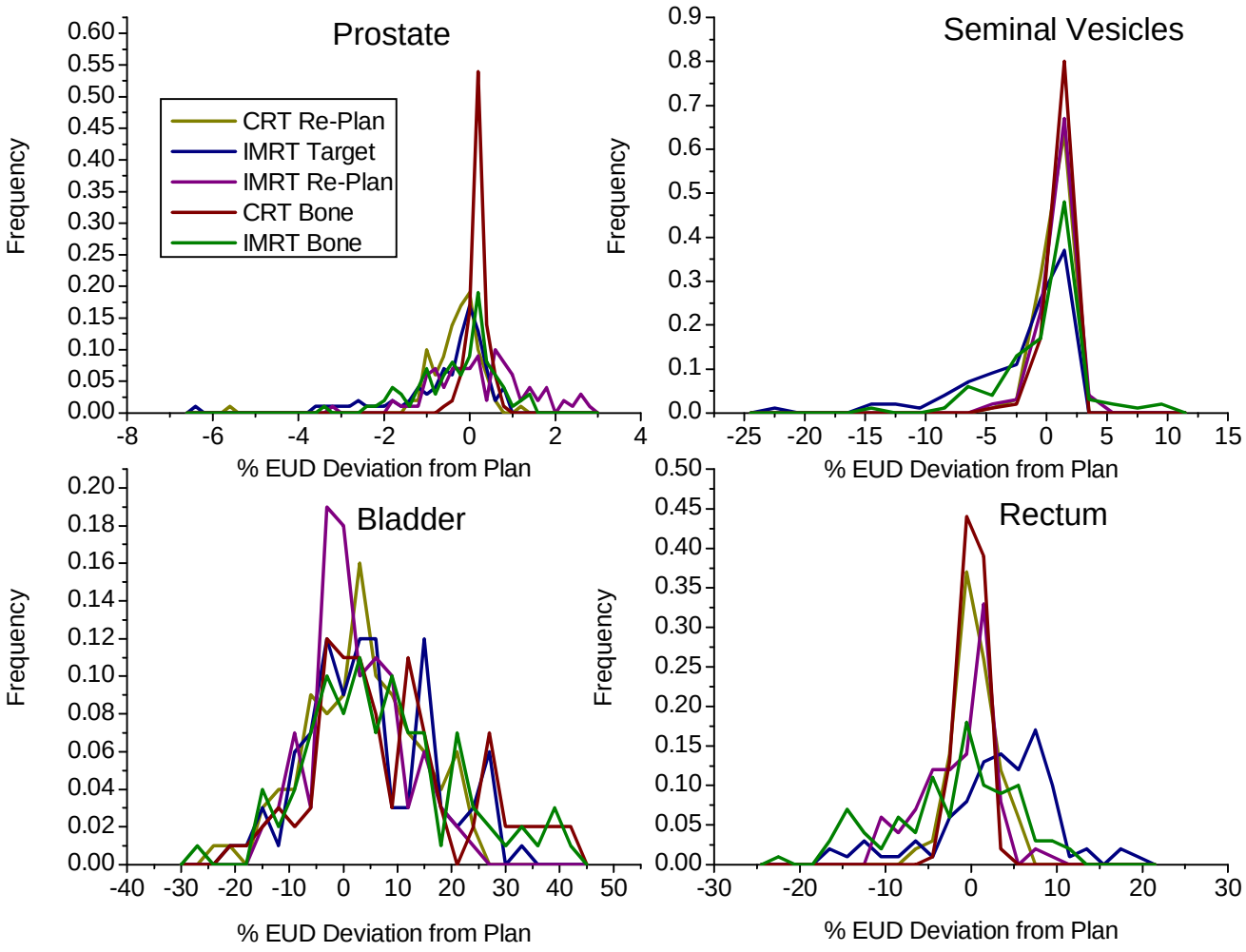

Figure 4 Histogram of individual fraction deviations from planned EUD, expressed as percent of the respective organ planning dose. Total number of treatment fraction N is 90.

Figure 5

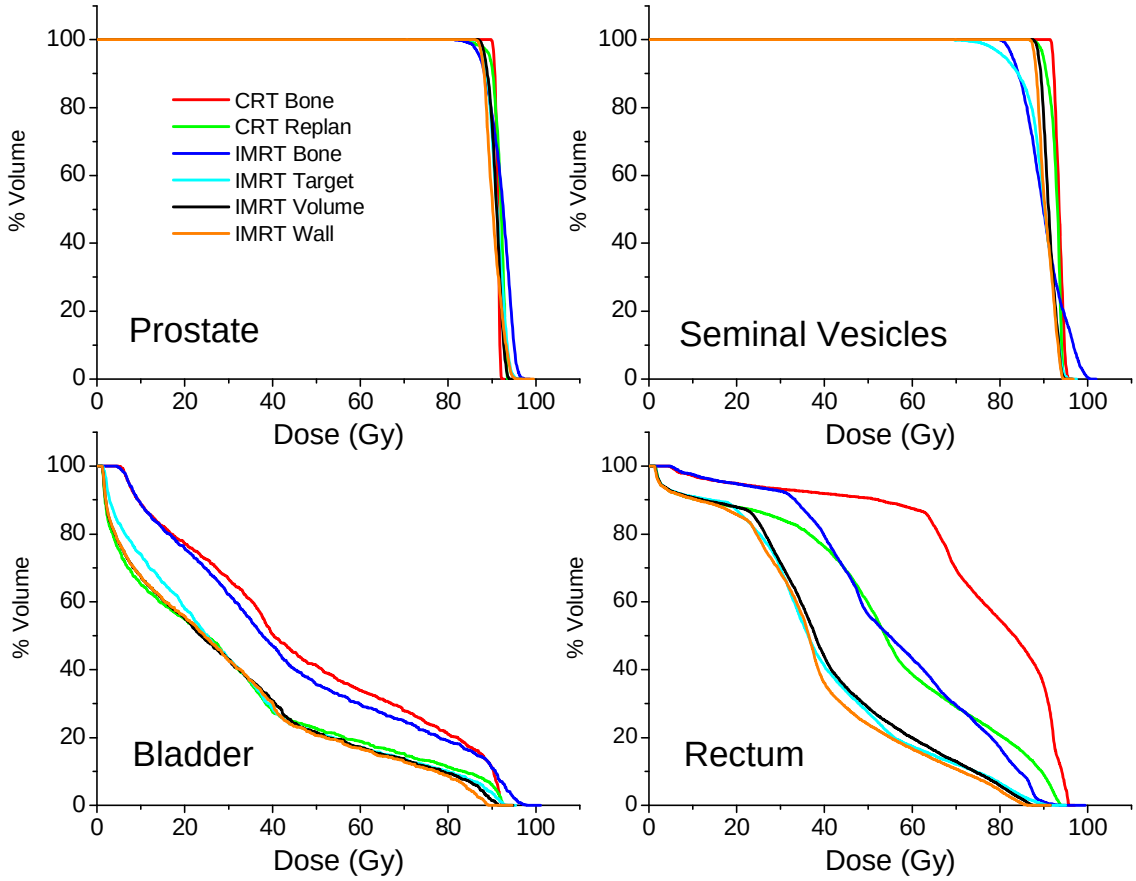

Figure 5. DVH of accumulated dose after 10 treatment fractions (patient #9).

Figure 6

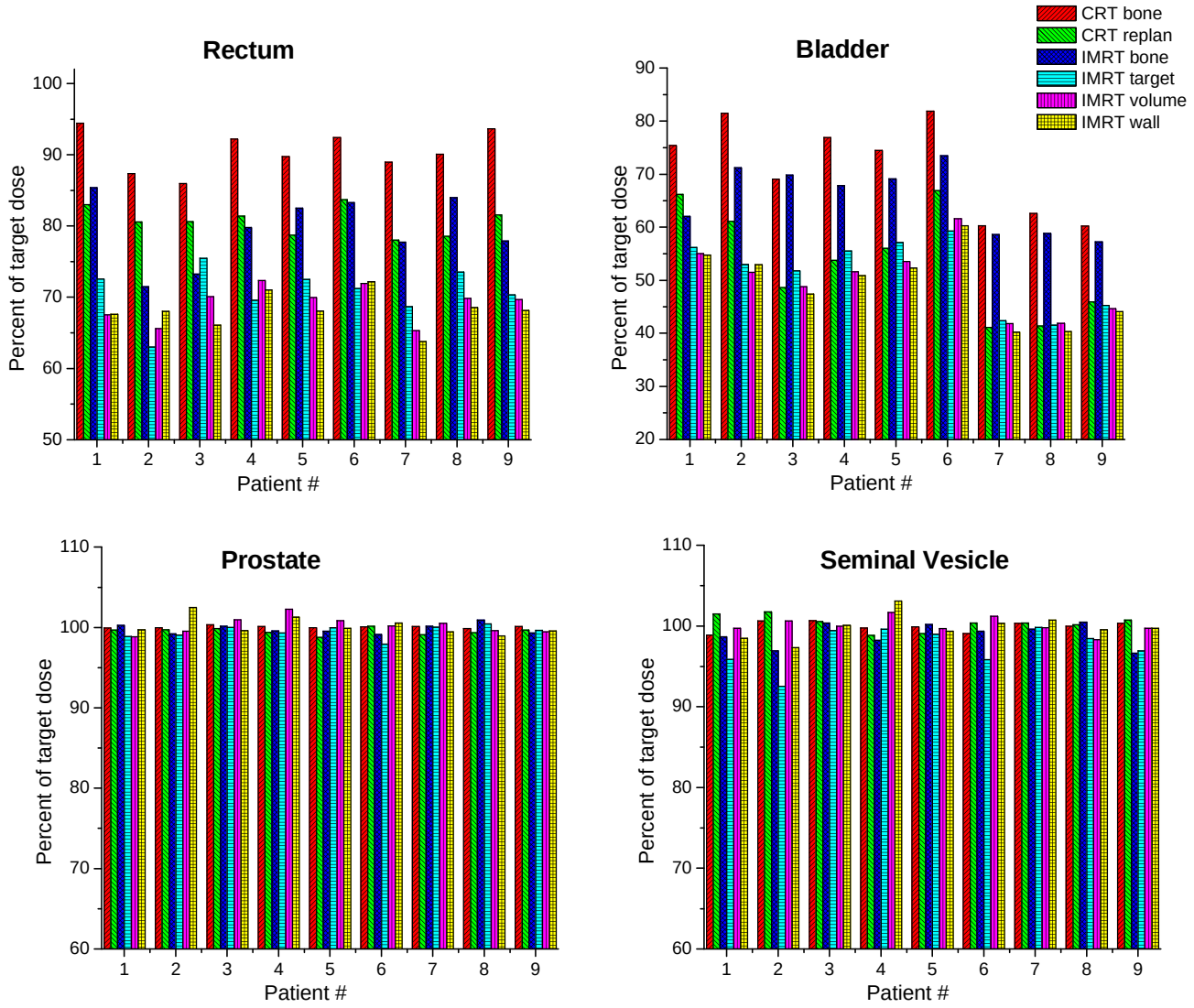

Figure 6 Accumulated EUD from 10 treatment fractions for different online IGRT strategies.

Figure 7

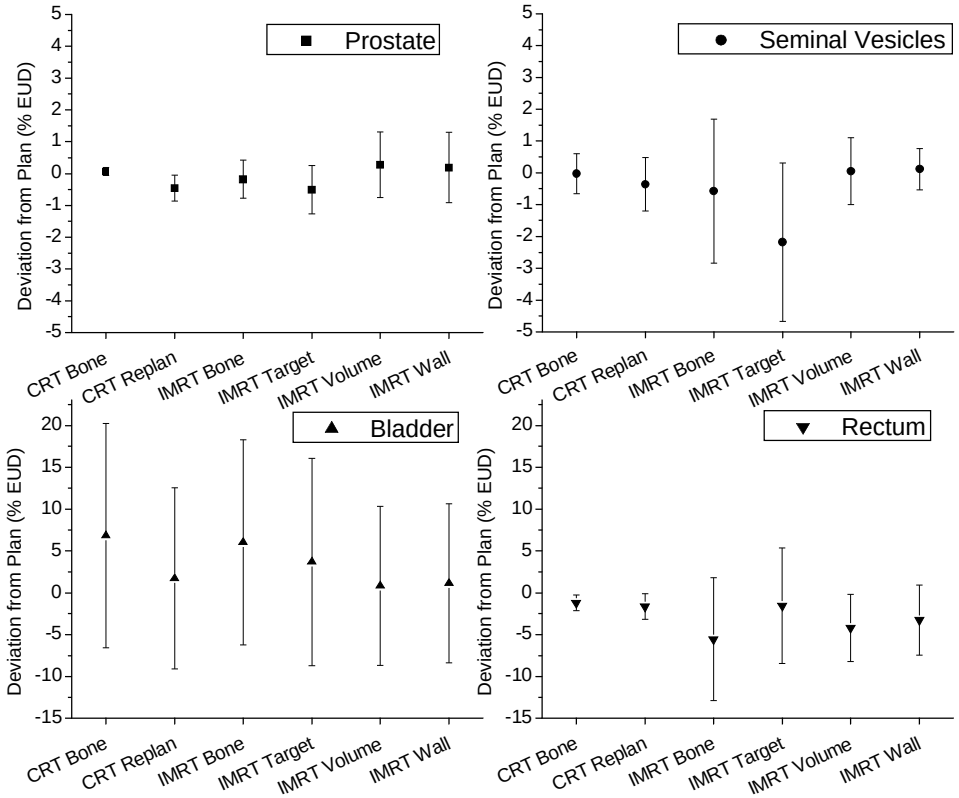

Figure 7 Discrepancies of cumulative delivered doses from treatment plan prediction, expressed as mean ± 1 standard deviation of all patients. The columns are the mean and the error bars are the standard deviation of the difference.